frontiers | Frontiers in Earth Science

TYPE Original Research
PUBLISHED 25 July 2024
DOI 10.3389/feart.2024.1416850

OPEN ACCESS

EDITED BY
Gang Rao,
Southwest Petroleum University, China

REVIEWED BY
Lei Wu,
Zhejiang University, China
Bin Deng,
Chengdu University of Technology, China

*CORRESPONDENCE
Shi Chen,
chenshi4714@163.com

RECEIVED 13 April 2024
ACCEPTED 04 July 2024
PUBLISHED 25 July 2024

CITATION
Song X, Chen S, Zhang Y, Xie Z, Neng Y, Liang X, Kang P, Yang M and Chen P (2024), New insights into the evolution and formation mechanism of SB5 fault: a case study from the Fuman Oilfield, Tarim basin, NW China. *Front. Earth Sci.* 12:1416850. doi: 10.3389/feart.2024.1416850

New insights into the evolution and formation mechanism of SB5 fault: a case study from the Fuman Oilfield, Tarim basin, NW China

Xingguo Song[1,2], Shi Chen[1,2]*, Yintao Zhang[3], Zhou Xie[3], Yuan Neng[1,4], Xinxin Liang[1,2], Pengfei Kang[3], Minghui Yang[1,2] and Ping Chen[1,2]

[1]National Key Laboratory of Petroleum Resources and Engineering, China University of Petroleum, Beijing, China, [2]College of Geosciences, China University of Petroleum, Beijing, China, [3]PetroChina Tarim Oilfield Company, Korla, China, [4]Department of Geoscience, China University of Petroleum at Karamay, Karamay, China

The Shunbei 5 (SB5) strike-slip fault, situated in the central Tarim basin, is distinguished by its considerable length, significant variations in planar orientation, and intricate multi-stage tectonic evolution. This study delves into the geometric, kinematic, and dynamic features of both the southern and northern parts of the SB5 fault, utilizing the latest seismic data from the Fuman Oilfield, and examines the factors influencing the fault's planar deflection. The fault can be categorized into three structural deformation layers based on lithological features and fault features: the deep structural deformation layer (below $T\epsilon_3$), characterized by basement rifting and limited strike-slip activity; the middle structural deformation layer ($T\epsilon_3$-TO_3), marked by vigorous strike-slip movements and the dominance of flower structures; and the shallow structural deformation layer (TO_3-TP), featuring echelon-type normal faults and boundary graben faults, specifically in the southern SB5 fault. The fault activity is more pronounced in its southern SB5 fault compared to the northern, with the weakest activity at the $T\epsilon_3$ interface and the peak at the TO_3 interface. The southern SB5 fault transitions to sinistral slip at the TO_3 interface, while the northern SB5 fault shifts from dextral to sinistral slip at the TC interface, highlighting variable slip directions across different interfaces. Rifts are extensively distributed within the Precambrian basement along the SB5 fault. The initial strike-slip fault rupture, which is primarily localized in these areas, exerts a significant influence on the formation of the S-shaped fault plane. This process involves four distinct evolution stages: the embryonic stage of strike-slip activity during the Middle-Late Cambrian; the intense strike-slip fault activity stage during the Middle-Late Ordovician; the reactivation stage of deep strike-slip fault in the Silurian; and the connection and reactivation stage during the Devonian-Carboniferous.

KEYWORDS

SB5 strike-slip faults, layered deformation, fault evolution, basement structure, formation mechanism, the tarim basin

1 Introduction

In recent years, with the continuous breakthroughs and innovations in geophysical technology, a series of strike-slip faults have been identified in the deep (4,500–6,000 m) and ultra-deep (>6,000 m) (Dyman et al., 2002) Paleozoic strata of the central Tarim Basin (Lan et al., 2015; Wu et al., 2016; Wu et al., 2020). In contrast to the large strike-slip faults located at plate boundaries, the strike-slip faults within the central Tarim Basin exhibit shorter lengths (mostly less than 50 km) and smaller displacement in map view (less than 2 km) (Han et al., 2017; Han et al., 2020; Deng et al., 2019a), and are classified as intracratonic strike-slip faults (Harding, 1974; Mann, 2007).

The strike-slip fault system is extensively distributed around the Manjiaer Depression, a region renowned for significant hydrocarbon finds within Paleozoic carbonate strata (Jiao, 2017; Tian et al., 2021; Deng et al., 2022). These discoveries include the Halahatang and Tahe Oilfields within the Tabei uplift, the Tazhong condensate gasfield in the Tazhong uplift, and the Shunbei and Fuman Oilfields located in the Manxi Low uplift. The strike-slip fault system is pivotal in oil and gas exploration and development, and its intricate developmental features have attracted considerable academic interest and sparked extensive scholarly investigation (Wang et al., 2016; Deng et al., 2018; Deng et al., 2019a; Deng et al., 2022; Wu et al., 2019a).

The SB5 fault extends across the Tazhong and Tabei Uplifts, marked by numerous oil and gas exploration discoveries, significant deformation magnitude, and an extensive longitudinal reach of approximately 270 km (Deng et al., 2019b). The fault stands as the longest strike-slip fault in the central Tarim basin, having emerged as a significant focus of academic research in recent years. Predecessors have carried out detailed research work on the SB5 fault, focusing on the layered deformation, staged evolution, segmentation, and fault-controlled carbonate reservoir (Teng et al., 2020; Wang et al., 2020; Sun et al., 2021; Liu et al., 2023; Yao et al., 2023). A model proposing the initial independent development of the northern and southern SB5 faults, followed by their connection in subsequent stages, has been put forward (Deng et al., 2019a; Deng et al., 2019b; Sun et al., 2021; Chen et al., 2023). Additionally, the evolutionary process of the fault plane morphology has been reconstructed (Sun et al., 2021; Yun, 2021). However, the earliest active period of SB5 fault and the specific division of active stages are still controversial. While the majority of scholars concur that fault activity commenced during the Middle to late Ordovician (Deng et al., 2019b; Shen et al., 2022), others propose activity in the Cambrian (Teng et al., 2020; Liu et al., 2023) and Early Ordovician (Chen et al., 2023). The SB5 fault's pronounced large-angle deflection along its strike has garnered widespread attention (Deng et al., 2018; Deng et al., 2019a; Wang et al., 2020; Sun et al., 2021), yet the underlying control factors remain obscure. The Precambrian basement rifts, extensively distributed across the basin (Neng et al., 2022), are known to exert significant control over the development of strike-slip faults in the Tazhong Uplift (Han et al., 2017). However, their influence on the development and evolution of the SB5 fault is still limited.

Drawing upon the latest 3D seismic data provided by the Fuman Oilfield, this article performs a comprehensive seismic interpretation, specifically focusing on the transitional zone connecting the northern and southern SB5 fault. The objectives of this study are as follows: 1) to elucidate and compare the spatial distribution characteristics of the southern and northern SB5 fault, 2) to re-evaluate the fault's earliest active period and delineate the phases of deformation, 3) to examine the attributes of the Precambrian basement structure underlying the SB5 fault and evaluate its influence on fault evolution, and 4) to delve into the controlling factors of the deflection of the SB5 fault.

2 Regional geological setting

The Tarim Basin, situated in northwest China, is the largest petroliferous superimposed basin in the country (Jia and Wei, 2002; He et al., 2005; He et al., 2006). It covers a vast area of about 560,000 km^2 (Tang, 1994; Jia, 1997). The basin is positioned between the Paleo-Asian and the Tethys tectonic domain (Allen et al., 1993; Lin et al., 2011; Lin et al., 2012), and is characterized by a complex surrounding tectonic environment. The Tianshan mountains are developed in the north, and the Kunlun Mountains and Altun Mountains surround the southwest and southeast, respectively. Based on the sedimentary characteristics and variations in basement structure, the Tarim Basin is segmented into 13 distinct tectonic units (Figure 1). The SB5 fault is located in the middle of the Tarim Basin, stretching through Manxi Low Uplift and linking Tabei Uplift with Tazhong Uplift. The principal region of the Fuman Oilfield is nestled within the Manxi Low Uplift, bordering the Tabei Uplift to the north and extending towards the Awati Depression to the west and the Manjiaer Depression to the east (Figure 2).

The tectonic evolution of the Tarim Basin is intricate, influenced by the activities of the surrounding orogenic belts. Following the breakup of the Rodinia supercontinent, the Tarim block emerged, giving rise to the Archean-Neoproterozoic early crystalline basement (Zhang et al., 2007; Wu et al., 2018). Paleo-oceans encircled the block, including the South Tianshan Ocean to the north, the ancient Kunlun Ocean to the southwest, and the Altun Ocean to the southeast (Mattern and Schneider, 2000; Li et al., 2009; Zhang et al., 2009). The tectonic setting of the basin is characterized as a passive continental margin, experiencing an overall extensional stress environment that persisted from the Precambrian through the early Ordovician (Li et al., 2013; Gao and Fan, 2014). In the middle and late Ordovician, the ancient Kunlun Ocean and Altun Ocean initiated gradual subduction beneath the Tarim plate (Zhang et al., 2002; Li et al., 2009), leading to a tectonic shift. The Altun tectonic domain experienced intense folding orogeny in the Silurian (Yang et al., 2005; Liu et al., 2007), prompting a transition in the basin's tectonic environment from extensional to compressional, during which the Tabei and Tazhong uplifts were formed (Wang, 2004; Ren et al., 2011). The south Tianshan Ocean in the north gradually closed from east to west in the Silurian in a scissors form, and finally closed in the Carboniferous (Allen et al., 1993; Gao et al., 2006; Han et al., 2011). By the Permian, the surrounding oceans had closed, and the Tarim Basin transformed into an intracontinental depression basin (Yang et al., 2005). Volcanic rocks spread extensively across the basin, influenced by the large igneous province (Sharps et al., 1989; Li et al., 2011; Xu et al., 2021). In the Triassic, the basin was subject to strong compression, with

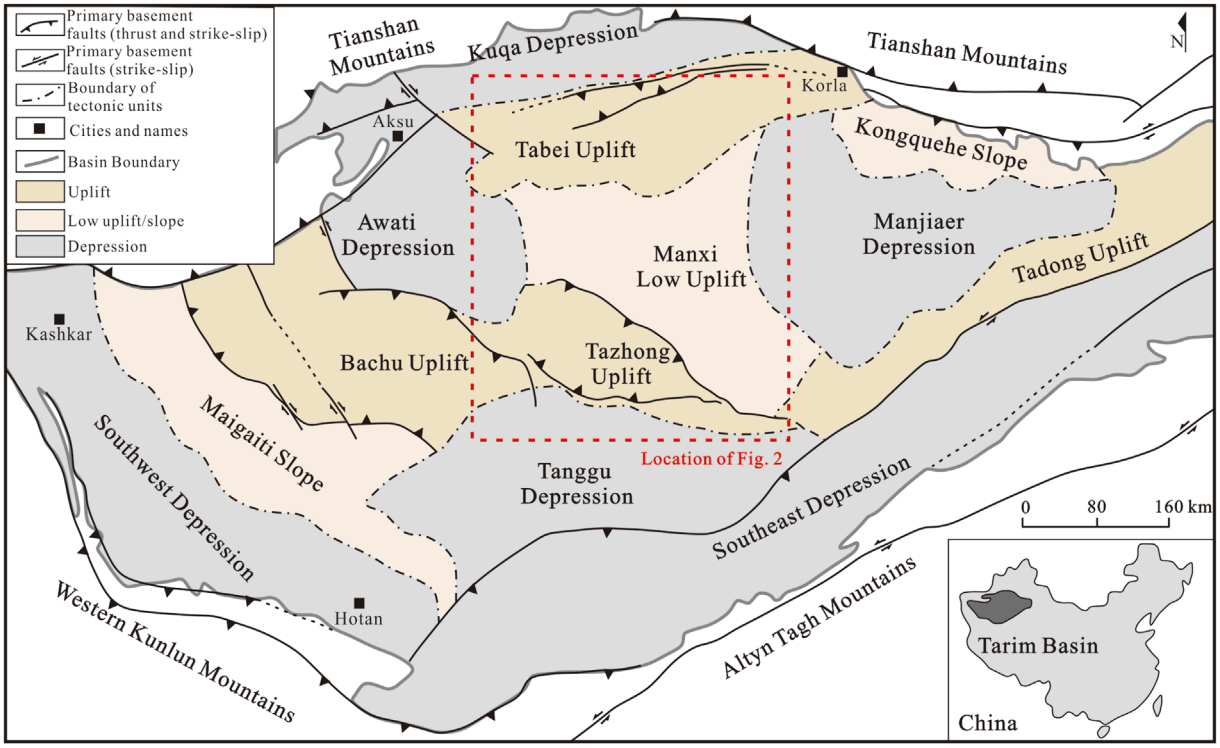

FIGURE 1
Simplified distribution map of the tectonic units in the Tarim Basin [modified from Li et al. (2013); Deng et al. (2019a)].

significant uplift and erosion due to the tectonic activity associated with the Paleo-Tethys block in the south (Yu et al., 2014). During the Jurassic, the basin experienced a period of weak extension. Zhang et al. (2007); Zheng et al. (2014). The Cenozoic era saw pronounced uplift and denudation within the basin, a result of the far-field effects from the collision between the Indian and Eurasian plates (Windley et al., 1990; Li et al., 2012; Zhu et al., 2022). This collision-induced uplift and erosion have continued to shape the geological and morphological features of the Tarim Basin into its present form.

The strata of the Tarim Basin are well developed, encompassing from the Proterozoic to Cenozoic, and the strike-slip faults are primary situated in the Paleozoic (Figure 3) (Deng et al., 2018). The Paleozoic strata were predominantly deposited in a marine sedimentary environment (Neng et al., 2022). The strata ranging from the Cambrian to the Middle Ordovician are primarily made up of carbonate rocks, with a distinctive Middle Cambrian layer known for its gypsum-salt rock. In contrast, the Upper Ordovician to Carboniferous strata are predominantly classified as clastic rocks, reflecting a shift in depositional environments. The Permian saw an extensive distribution of igneous rocks, indicating significant tectonic and magmatic activity. The hydrocarbon exploration discoveries related to strike-slip faults in the basin are mainly concentrated in the Yijianfang and Yingshan formation of the Lower-to-Middle Ordovician (Li et al., 2019; Tian et al., 2021; Wang et al., 2021). These reservoirs are characterized as fault-controlled fracture-cave, with the Yuertus formation of the Lower Cambrian serving as the primary source rock. The Upper Ordovician mudstones serve as effective regional seal (Ma et al., 2019; Deng et al., 2022). The Cambrian subsalt trap holds significant potential for oil and gas exploration (Yang et al., 2020; Zhu et al., 2022a; Zhu et al., 2022b). Effective reservoirs have already been identified within the dolomite strata of the Wusonggeer and Xiaoerbulake formations in the Lower Cambrian. In addition, the thick gypsum-salt layers of the Middle Cambrian have proven to be effective caprock, enhancing the potential for hydrocarbon accumulation and discovery within the Tarim Basin.

The Paleozoic ultra-deep strike-slip fault system in the Tarim Basin exhibits intricate features in plane view, revealing typical characteristics of differential development zones. It has been categorized into three tectonic deformation zones: Tabei Uplift, Manxi Low Uplift, and Tazhong Uplift (Figure 2). NW-trending faults are primarily developed in the Tabei uplift to the west of the SB5 fault, while two groups of small-angle X-type faults are present in the east of the SB5 fault. The Manxi Low Uplift to the west of the SB5 fault exhibits a consistent pattern of NW-trending faults, while the eastern part is marked by NE-trending faults, forming a distinctive broom-shaped distribution. The Tazhong Uplift in the west of the SB5 fault is characterized by NW-trending faults, whereas the east features a predominantly NE-oriented arrangement of strike-slip faults. These faults are parallel and intersect perpendicularly with thrust faults, contributing to the structural complexity of the area. Additionally, NEE-trending faults emerge in the southeast, forming conjugate systems with the NE-trending faults.

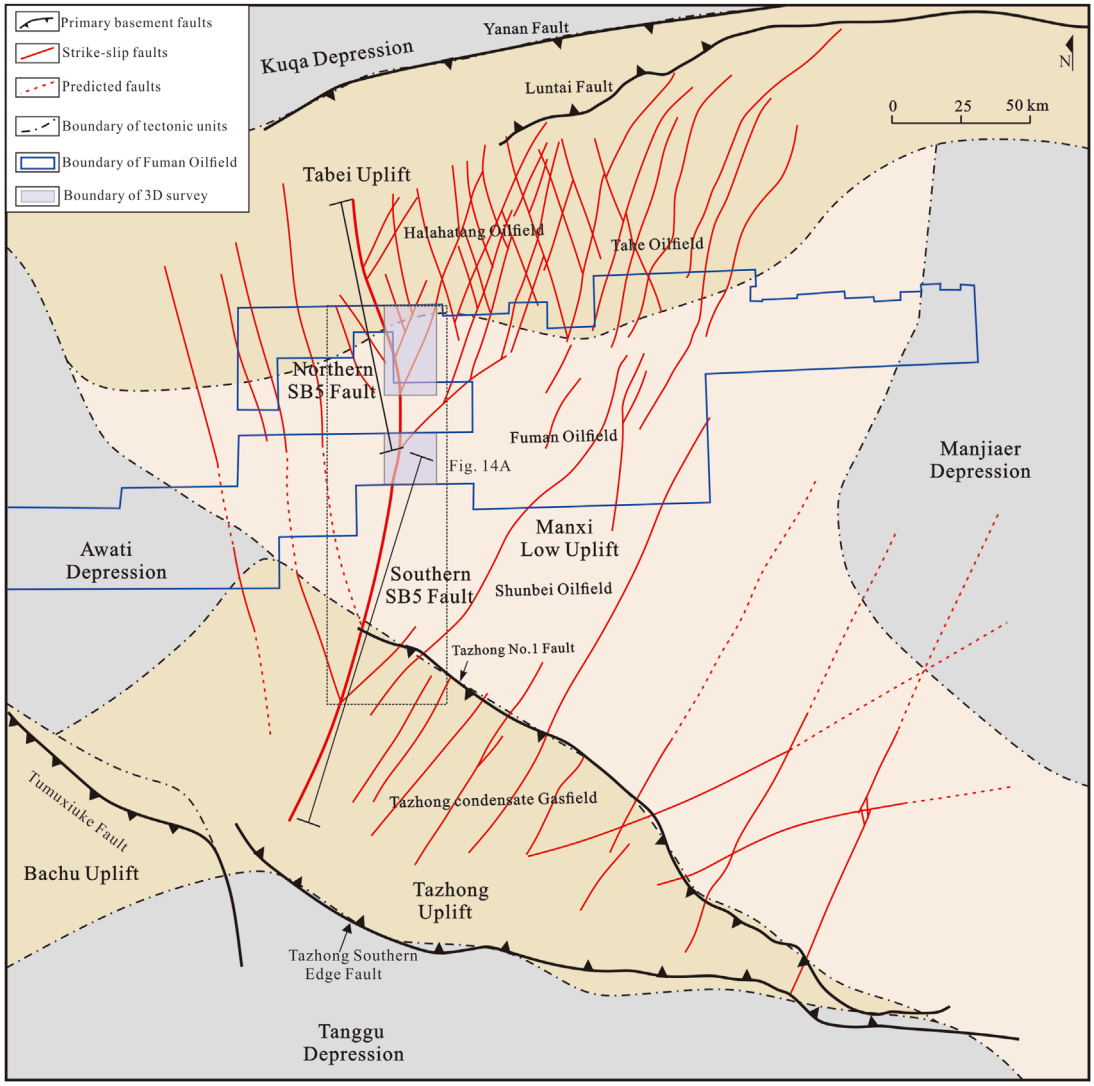

FIGURE 2
Enlarged view of the northern part of Figure 1, simplified tectonic map showing the major tectonic units and fault distribution in the central Tarim Basin (revised after Deng et al., 2019a; Wang et al., 2020; Chen et al., 2024).

3 Data and methods

The high-precision 3D seismic data used in this study are provided by China National Petroleum Corporation (CNPC), including two 3D suvery, located in the west of Fuman Oilfield (Figure 1).

3D seismic data is interpreted by landmark software. Combined with the well logging data and the well-seismic correction, the seismic reflection interface of the crucial layers is calibrated. These include $T\epsilon_1$, $T\epsilon_2$, $T\epsilon_3$, TO, TO_3, TS, TD, TC, TP, which represent the bottoms of the Lower Cambrian, Middle Cambrian, Upper Cambrian, the bottom of the Ordovician, Middle Ordovician, Silurian, Devonian, Carboniferous and Permian. A grid for interpretation has been applied, with a spacing of 200 m × 200 m, aligned along the north- and east-respectively. Based on the statistics of vertical separation, the width of the deformation zone, and fault throw (Figures 4A, B), the fault activity in varied layers along the SB5 fault's strike can be analyzed on the seismic profile. The slip directions of strike-slip faults in different periods can be restored by extracting horizon depth slices near the crucial layers ($T\epsilon_3$ and TO_3) and analyzing the arrangement of secondary faults (Han et al., 2017; Deng et al., 2019a). Furthermore, the distribution characteristics of the Precambrian basement rift in the study area can be restored by depicting the bottom surface of the Sinian in the profile, and the controlling effect of the basement on the SB5 fault can be analyzed.

4 Geometric characteristics of SB5 fault

SB5 fault is situated in the central Tarim Basin, passing through Manxi low uplift and connecting Tazhong uplift and Tabei uplift

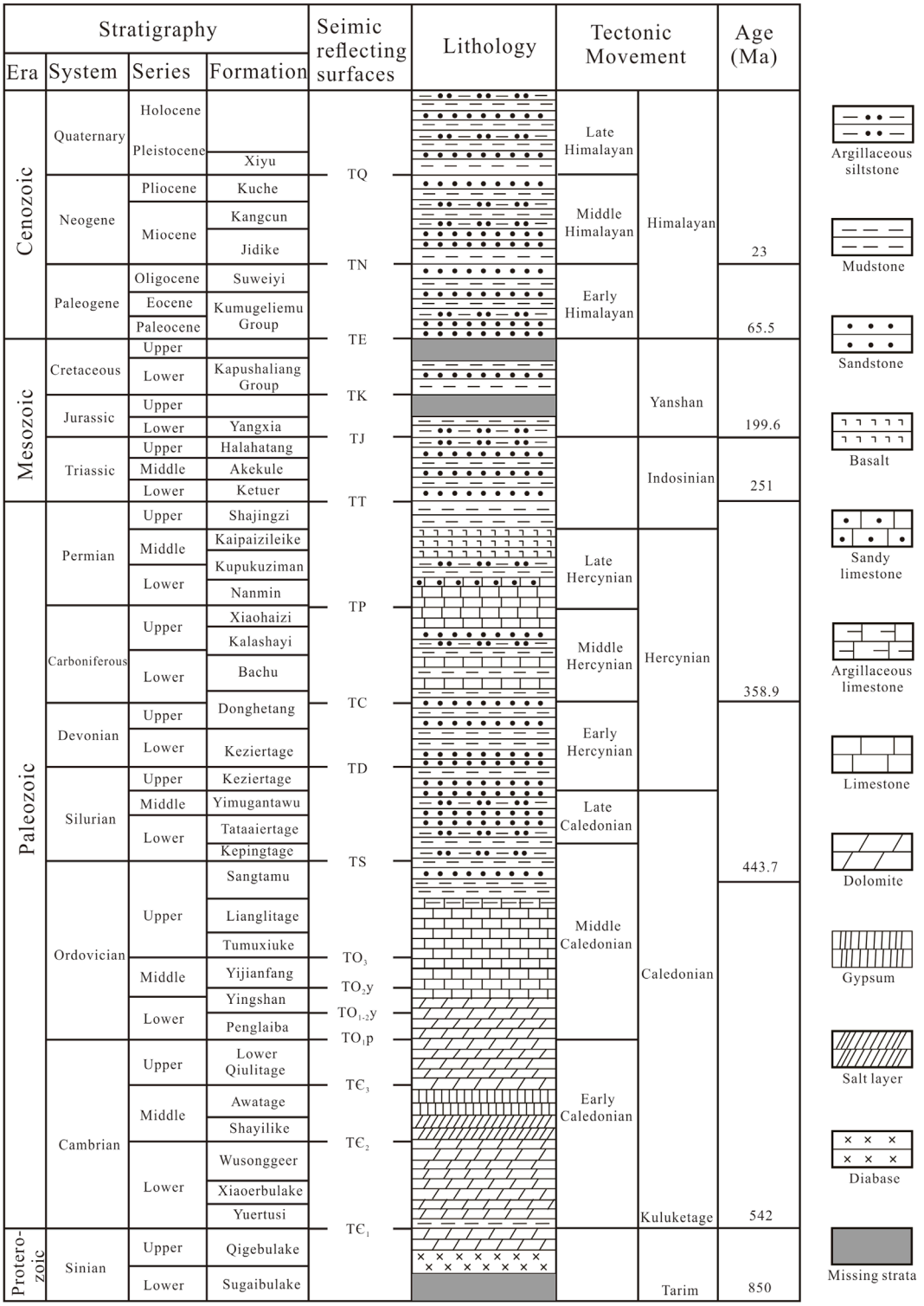

FIGURE 3
Chart showing the Tarim Basin stratigraphy, the seismic reflecting surfaces (horizons), and the timing of regional tectonic movements [modified from Deng et al. (2019b); Neng et al. (2022)].

(Deng et al., 2019b). The plane shape of the fault is curvilinear and deflects clockwise from north to south. Taking the intersection with SB1 fault as the boundary, it can be divided into northern and southern SB5 fault according to the strike characteristics. In particular, the main strike of the northern SB5 fault is NNW, while that of the southern SB5 fault is NNE, consistent with the

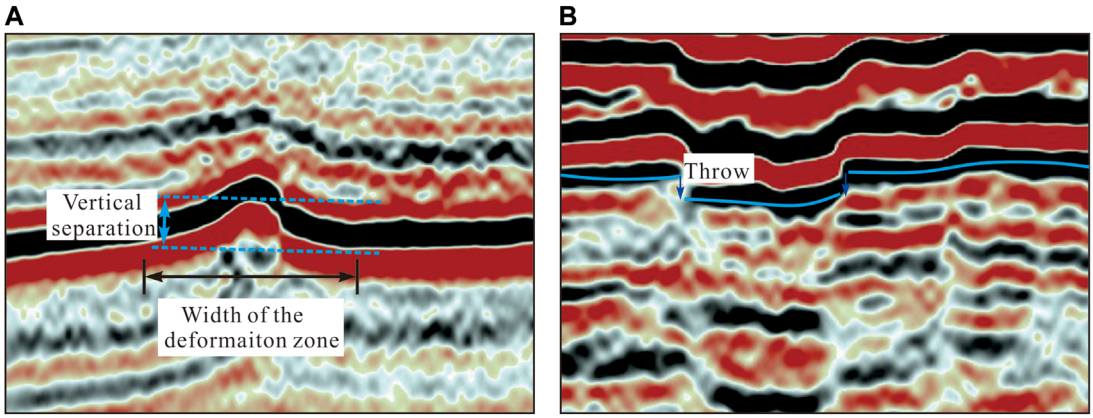

FIGURE 4
Typical seismic sections illustrating **(A)** the vertical separation, width of deformation zone, and **(B)** fault throw.

characteristics of strike-slip fault systems in Tabei and Tazhong uplift respectively (Figure 2). Fuman Oilfield's 3D surveys encompass the junction of the northern and southern SB5 fault, spanning approximately 53 km in length. Through the detailed interpretation of three-dimensional seismic data, the plane and profile characteristics of the northern and southern SB5 fault are shown and compared.

4.1 Geometry of SB5 fault in plane view

Based on the connection modes between faults, the transfer zones are divided into two types: hard linkage and soft linkage (Gupta and Scholz, 2000). The soft linkage transfer zone is characterized by overlapping faults that have not yet connected directly. Initially segmented faults progressively integrate into a larger fault system, where hard linkage transfer zones emerge at the fault's bending junctions.

The SB5 fault exhibits significant variations in the plane characteristics across shallow and deep interfaces. The coherence of $T\epsilon_1$ (Figure 5A) reveals that the faults primarily develop in linear features. The fault segments overlap through soft linkages. In the northern SB5 fault, the overlap of smaller fault segments is prominent, typically ranging from 2 to 3 km, with locally discontinuous fault segment connections. In contrast, the fault development in the southern SB5 fault is more intricate, exhibiting longer fault segment and larger overlap lengths, reaching 5–6 km, and greater overlap widths.

The coherence of $T\epsilon_3$ indicates that the faults exhibit more prominent linear characteristics compared to $T\epsilon_1$, accompanied by elongated fault segment lengths (Figure 5B). Furthermore, hard linkages develop between fault segments, and the intersection points with neighboring faults exhibit intricate fault development patterns, such as rhomboid overlaps. The primary distinction between the northern and southern SB5 fault lies in the development of strike-slip-derived structures within the deformation zones, where branch faults are notably more densely distributed in the southern SB5 fault.

The coherence of TO_3 shows that the northern SB5 fault (Figure 5C) shares similar development characteristics with $T\epsilon_3$. However, the fault activity of the TO_3 is more intense, and the segment length is greater, ranging from 8 to 10 km. The fault overlaps in the form of hard linkages, exhibiting braided structures, rhombic overlapping patterns, and parallel overlapping configurations. There are boundary grabens on both sides of the southern SB5 fault (Figure 5C), which share strike with the strike-slip faults and extend to the junction of SB1 fault.

The coherence of TS reveals the presence of echelon normal faults (Figure 5D). The echelon normal fault in the northern SB5 fault is arranged in the left-step, with fault strikes range from 20° to 45°. Boundary grabens continue to develop on both sides of the southern SB5 fault, while echelon faults are present within the graben normal faults, with strike in NW direction and arranged in the right-step along the underlying strike slip faults.

The coherence of TC reveals the presence of echelon normal faults in both the northern and southern SB5 fault; they are arranged in a right-step pattern with a primary strike direction in NW (Figure 5E). In comparison to the northern SB5 fault, the echelon normal fault in the southern SB5 fault exhibits a denser development, longer individual fault segments and a more pronounced coherence attribute.

4.2 Structural styles in sections

The SB5 fault section exhibits distinct characteristics of layered deformation structure, encompassing multiple structural deformation layers arranged from deep to shallow (Deng et al., 2019a; Sun et al., 2021). In this study, the fault is categorized into three distinct structural deformation layers based on the characteristics of fault deformation and lithological interfaces (Figure 6), including deep structural deformation layer (below

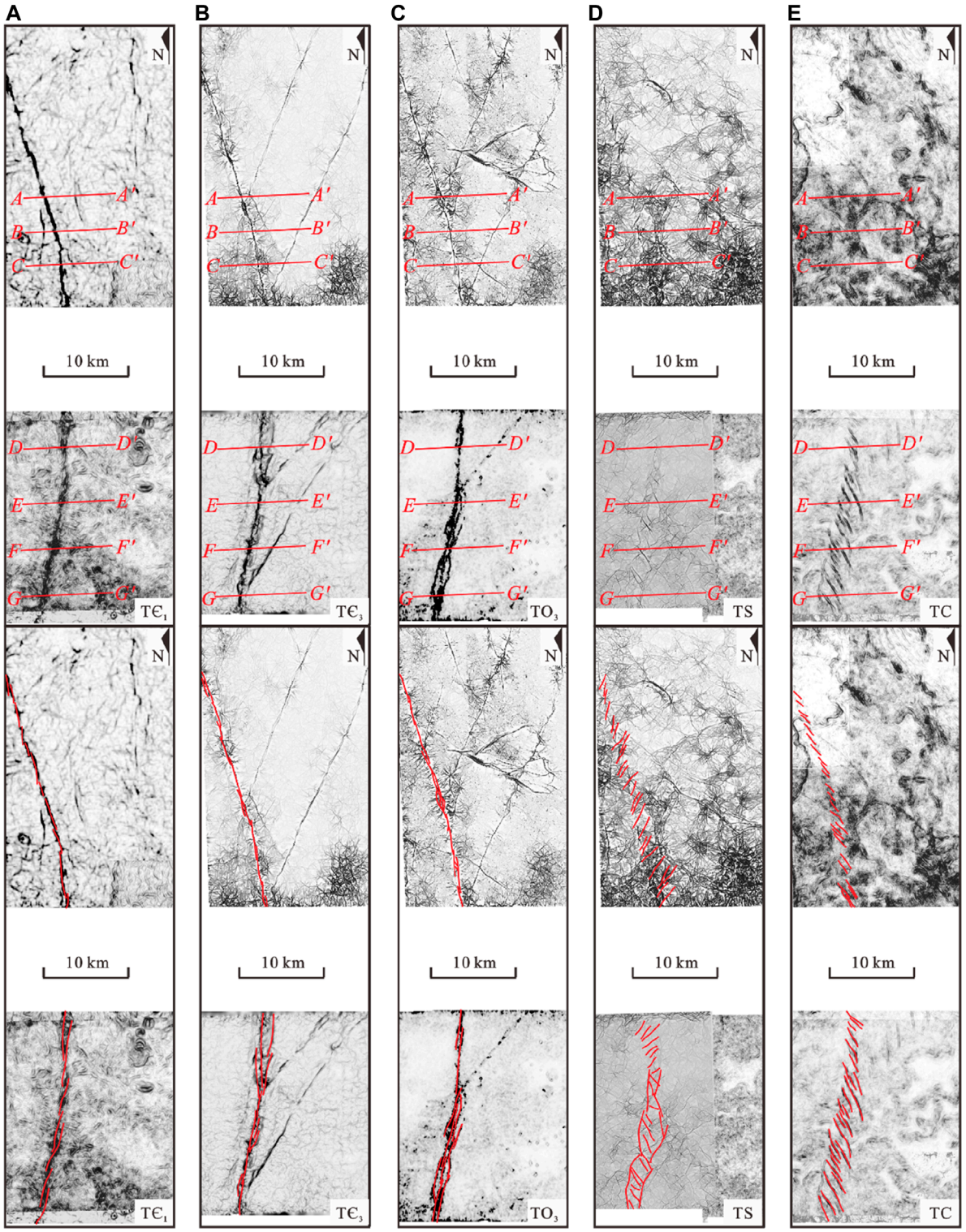

FIGURE 5
Uninterpreted (upper) and interpreted (lower) coherence slices of the **(A)** $T\epsilon_1$, **(B)** $T\epsilon_3$, **(C)** TO_3, **(D)** TS, and **(E)** TC seismic surfaces covering the NSB5FZ and SSB5FZ in Fuman oilfield. **(A)** On the $T\epsilon_1$ interface, the faults primarily develop in linear features, with segments overlap through soft linkages. **(B)** On the $T\epsilon_3$ interface, the faults exhibit more prominent linear characteristics compared to $T\epsilon_1$, accompanied by elongated fault segment lengths. **(C)** On the TO_3 interface, the fault overlaps in the form of hard linkages, exhibiting braided structures, rhombic overlapping patterns, and parallel overlapping configurations. **(D)** On the TS interface, echelon normal faults are arranged in the left- and right-step in the northern and southern SB5 fault respectively, while boundary graben faults develop along the southern SB5 fault. **(E)** On the TC interface, echelon normal faults are arranged in a right-step pattern. (see Figure 2 for the location of 3D survey).

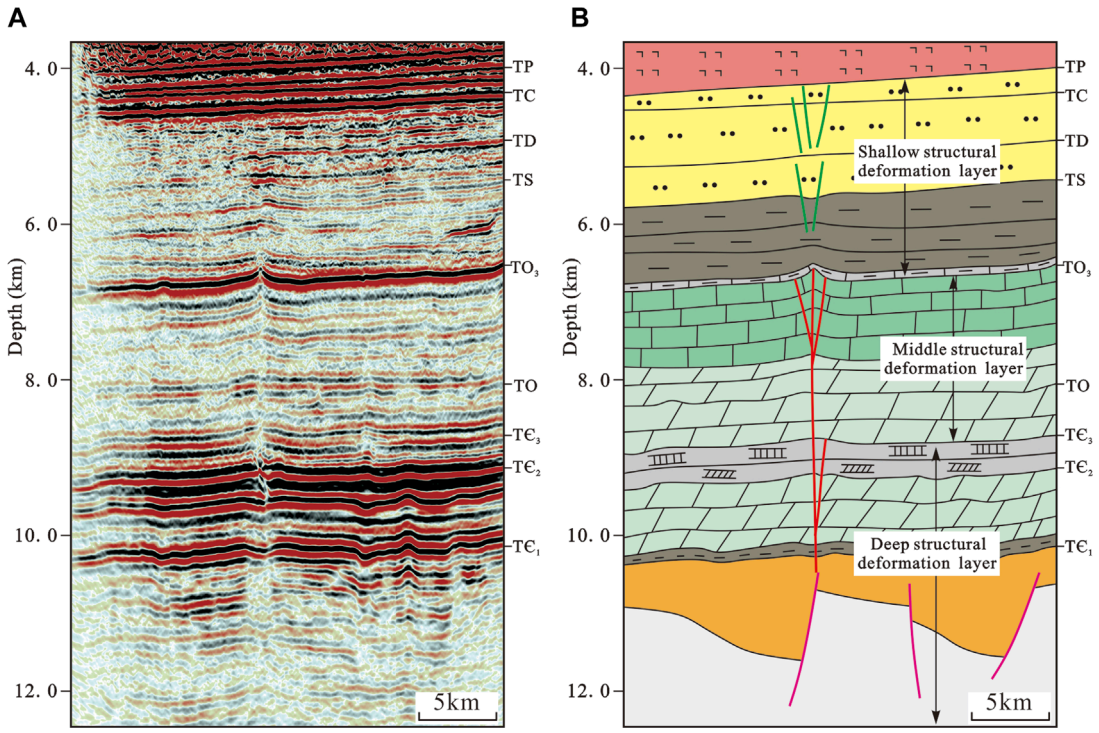

FIGURE 6
Typical seimic profile **(A)** and layered Deformation Structure model **(B)** of the SB5 fault. Deep structural deformation layer (below TЄ3), middle structural deformation layer (TЄ3-TO3), and shallow structural deformation layer (TO3-TP).

$T\epsilon_3$), middle structural deformation layer ($T\epsilon_3$-TO_3), and shallow structural deformation layer (TO_3-TP). The deep structural deformation layer exhibits a distinct pattern of relatively weak strike-slip fault activity, accompanied by the prominent development of Precambrian basement paleo-uplifts and rift structures, which have been intersected by some ultra-deep boreholes (Zhu et al., 2017; Chen et al., 2022). The primary lithology within the middle structural deformation layer consists of carbonate rocks, with intense strike-slip fault activity. The shallow structural deformation layer is dominated by clastic rock, and it is characterized by the development of echelon normal faults following the reactivation of strike-slip faults.

4.2.1 Northern SB5 fault

In the northern SB5 fault, the basement rift structure is distinct in the deep structural layer. The strike-slip fault penetrates the basement vertically, primarily occurring along the boundary between the paleo-uplift and the rift (Figures 7A–C), or above the normal fault on the rift margin (Figures 7B–D). Strike-slip faults are upright, locally developed branch faults and terminated near the bottom of the Upper Cambrian ($T\epsilon_3$ interface) (Figure 7A), forming a semi-flower structure. Furthermore, the Middle Cambrian gypsum-salt layer underwent translation, transpression, and transtension, resulted in the formation of salt sheets (Figure 7A), salt anticlines (Figure 7B), and salt sag (Figure 7D).

The faults in the middle structural layer are intensely active near the bottom of the Upper Ordovician (TO_3). The strata experience significant fold deformation due to the development of multiple branch faults, which coalesce to form intricate flower-structures that are mostly positive (Figures 7A–D).

The development of normal faults in the shallow structural layer is extensive, leading to distinct fault offsets and the formation of graben and half-graben structures. Vertically, these echelon normal faults can be separated into upper and lower groups based on their distribution positions (Figures 7A–D). The normal fault of the lower group terminates upward beneath TD interface and extends downward into the Upper Ordovician, growth strata occurred in Silurian, but it generally does not traverse through TO_3 interface. The normal faults of the upper group are primarily distributed between interfaces of TP and TD, and there is synsedimentary thickening in both Devonian and Carboniferous.

4.2.2 Southern SB5 fault

In the southern SB5 fault, the deep structural layer exhibits similarities to that of the northern SB5 fault, with clear indications of Precambrian basement rift and paleo-uplift. The strike-slip faults vertically penetrate the basement, aligning along rift edges or above basement normal faults. Near the $T\epsilon_3$ interface, the southern SB5 fault shows a higher prevalence of branch faults, characterized by well-developed flower and semi-flower structures. Additionally, the Middle Cambrian gypsum-salt layer within the deformation zone experiences increased deformation, resulting in significant vertical

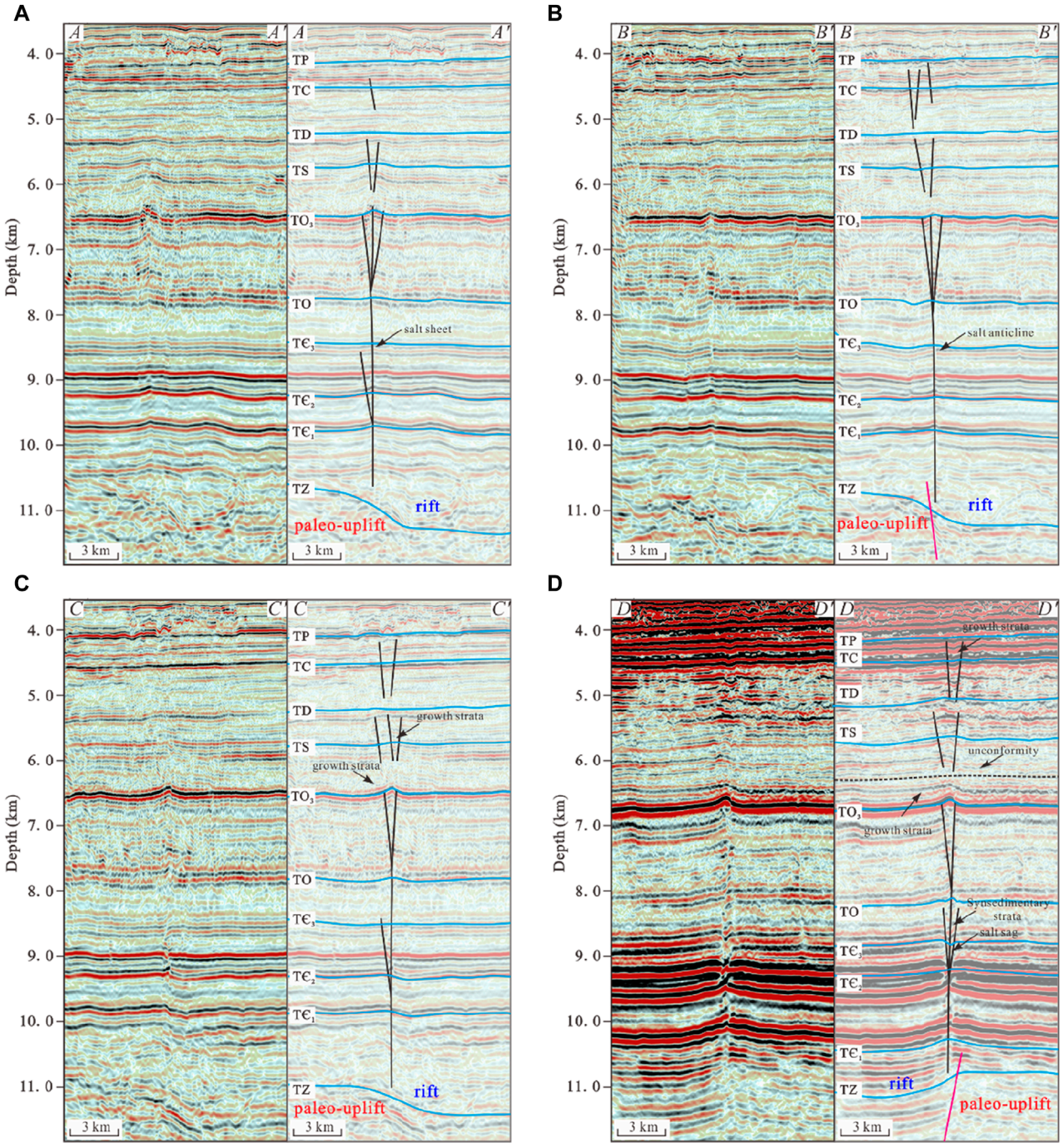

FIGURE 7
Uinterpreted (left) and interpreted (right) seismic cross sections of the northern SB5 fault **(A–D)**. (for location, see Figure 5)

displacement and the formation of distinct unconformities near the $T\epsilon_3$ interface (Figures 8A, B).

Within the middle structural layer, the boundary normal fault cuts through the interface of TO_3, while the main trunk of the strike-slip fault stands upright with branches flourishing on both sides, creating a complex flower structure. The strata present an overarching curved form, and the crest of the anticline experiences a downward fall. (Figures 8A–C).

In the shallow structural layer, normal faults can be categorized into two distinct groups. The lower group consists of normal faults that are primarily distributed within the Upper Ordovician and Silurian strata. These faults include boundary grabens characterized by significant fault displacement, as well as echelon normal faults that are interspersed across the graben region. A notable feature is the synsedimentary thickening observed in the Silurian strata within the graben (Figure 8A), which suggests active

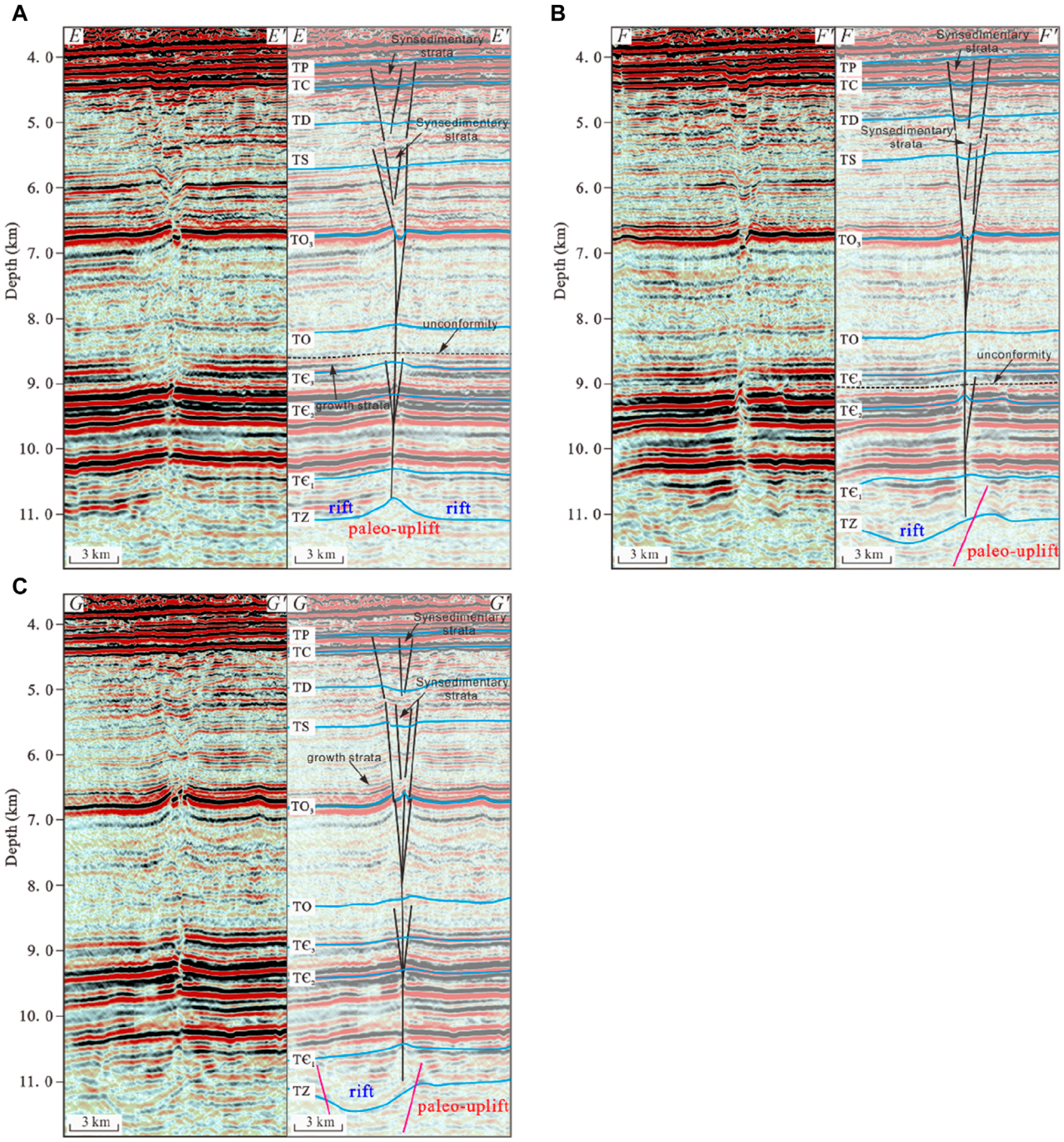

FIGURE 8
Uinterpreted (left) and interpreted (right) seismic cross sections of the southern SB5 fault **(A–C)**. (for location, see Figure 5)

faulting concurrent with sedimentation. The upper group of normal faults in the shallow structural layer shares analogous traits with those observed in the northern SB5 fault, and they terminate upwards at the interface of TP. However, these faults exhibit a heightened degree of activity and more pronounced fault displacement, as they extend further down into the Silurian strata. Additionally, there is a marked synsedimentary thickening within the Devonian and Carboniferous strata of the graben (Figures 8A–C).

5 Fault activity along the SB5 fault

5.1 Characteristics of fault deformational magnitude

By measuring the width of the deformation zone (Figures 9A, B), the vertical separation amplitude and the fault throw (Figures 10A, B), the characteristics of the fault deformational magnitude at critical interfaces can be compared and analyzed.

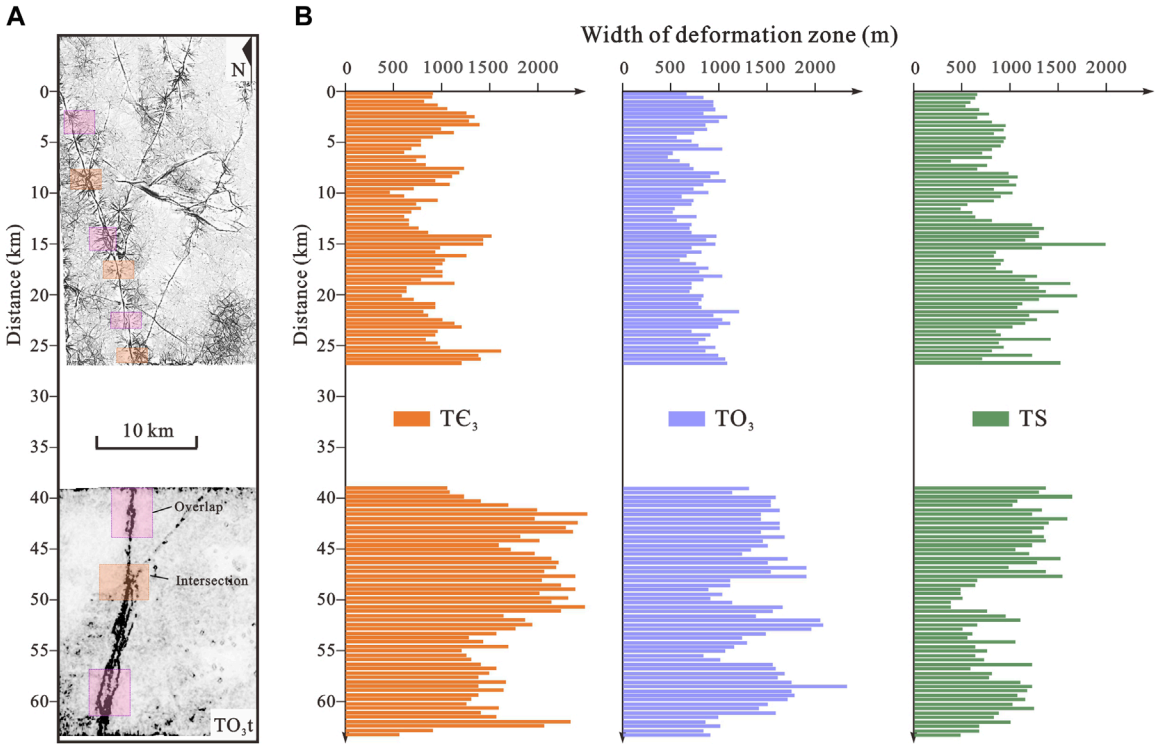

FIGURE 9
(A) Uninterpreted coherence slice of surface TO_3. **(B)** Histogram showing the width of deformation zone in surfaces of $T\epsilon_3$, TO_3, and TS. The widths of the deformation zones display consistent patterns across layers, with peak values occurring at segment overlaps and intersections with neighboring faults.

The width of the deformation zones (Figures 9A, B) reveal consistent patterns across layers, with peak values occurring at segment overlaps and intersections with neighboring faults. The vertical consistency suggests an inherited characteristic in the deformation zone widths. The $T\epsilon_3$ interface stands out with the most significant average deformation zone width, related to the high mobility and weaker competence of the Middle Cambrian gypsum-salt layer. The southern SB5 fault has a broader deformation zone compared to the northern SB5 fault, influenced by the variety of induced structures. At the TO_3 interface, the width of the fault deformation zone is found to be similar to that at the $T\epsilon_3$ interface, with the southern SB5 fault showing a wider deformation zone than its northern counterpart. On the TS interface, both the southern and northern SB5 faults display similar echelon normal fault development, but the southern SB5 fault is marked by large boundary grabens, contributing to wider deformation zone (Figure 5C).

The vertical separation amplitude and fault throw of the strata within the fault deformation zone (Figure 10B) serve as indicators of the fault's activity intensity. These characteristics demonstrate a pattern of vertical inheritance, with more pronounced deformation in areas where faults overlap and intersect with adjacent faults (Figures 10A, B). At interface of $T\epsilon_3$, the vertical separation amplitude is significantly greater in the southern SB5 fault than in the northern SB5 fault. The main area of the southern SB5 fault is characterized by uplift, while the northern SB5 fault shows a mix of uplift and subsidence. At the TO_3 interface, both southern and northern SB5 faults exhibit substantial vertical deformation, with the southern SB5 fault primarily marked by subsidence and the northern SB5 fault mainly by uplift. At the TS interface, the normal fault in the southern SB5 fault presents a larger fault throw than its northern counterpart, which may be ascribed to the presence of large boundary grabens.

5.2 Horizontal slip direction

Slip direction is a critical kinematic feature of faults, which is of great significance for the analysis of fault evolution and formation mechanism (Han et al., 2017; Deng et al., 2019a). The slip direction in the deep and middle structural layers is typically determined through horizontal depth slices. As for the echelon normal faults in the shallow structural layer, which arise from the reactivation of strike-slip faults, the slip direction can be inferred by examining the layout of these faults (Deng et al., 2018).

The slip direction of the SB5 fault displays a variability as it transitions from deeper to shallower layers. The depth slice of 3D seismic data reveals that the strike-slip faults have cut through and offset the strata, thus allowing for the determination of the fault's slip direction based on the characteristics of the stratigraphic offsets (Figures 11B, C). The slip direction of the southern SB5 fault on $T\epsilon_3$ aligns with that of the northern SB5 fault, both exhibiting a dextral movement pattern (Figure 11B). However, upon reaching the TO_3 interface, a shift occurs: the northern SB5 fault maintains dextral

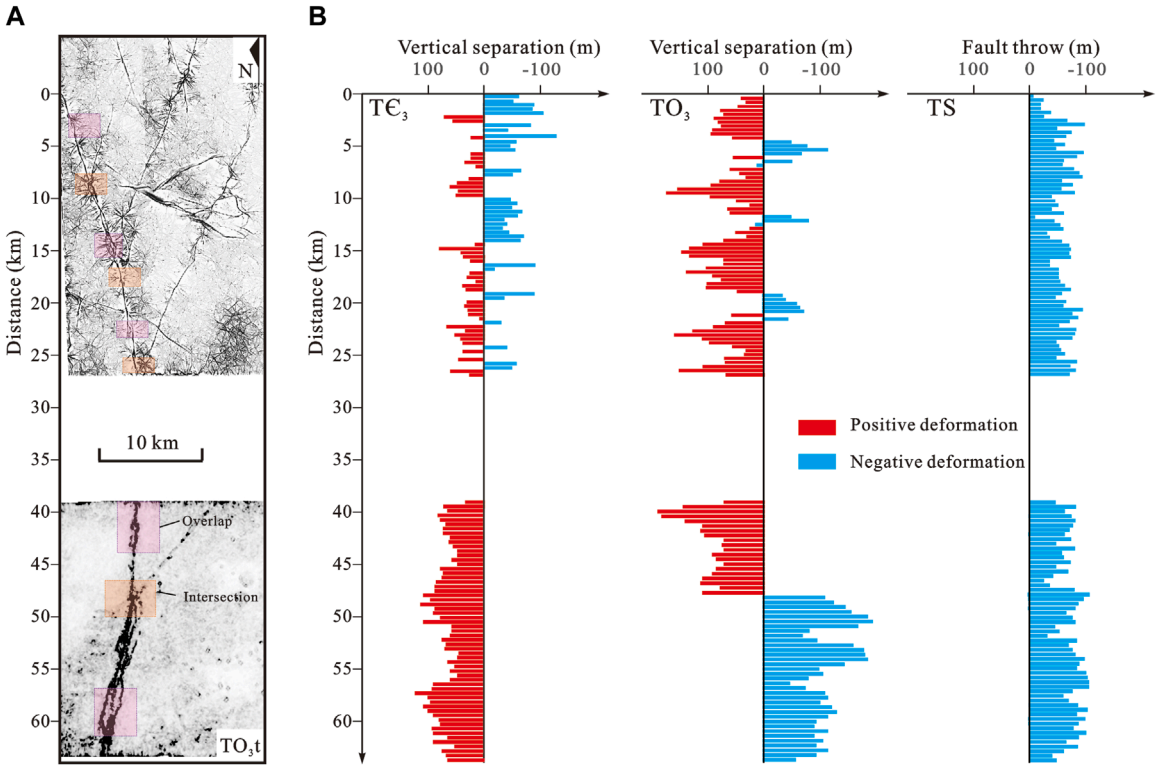

FIGURE 10
(A) Uninterpreted coherence slice of surface TO_3. **(B)** Histogram showing the vertical separation and fault throw in surfaces of $T\epsilon_3$, TO_3, and fault throw in TS. These characteristics demonstrate a pattern of vertical inheritance, with more pronounced deformation magnitude in areas where faults overlap and intersect with adjacent faults.

movement, while the slip direction of southern SB5 fault changes to sinistral (Figure 11C). The pattern of slip direction is consistent on the TS interface, aligning with the TO_3 interface (Figure 11D). On the interface of TC, the northern SB5 fault undergoes a reversal, matching the slip direction of the southern SB5 fault, which is characterized by sinistral movement (Figure 11E).

6 Discussion

6.1 Active stage of SB5 faults

Previous researchers have conducted a thorough investigation into the division of active stages of the SB5 fault, and the majority of scholars concur that the earliest active period of this strike-slip fault occurred during the Middle (Lin et al., 2021; Sun et al., 2021; Chen et al., 2023; Yao et al., 2023) and late Ordovician (Deng et al., 2019a; Deng et al., 2019b; Wang et al., 2020; Shen et al., 2022). However, the latest research shows that there was compressional tectonic stress in the Tarim basin during the Cambrian (Mattern and Schneider, 2000; Xu et al., 2011; Ge et al., 2014; Han et al., 2015), and the onset of strike-slip activity could be traced back to the Cambrian (Teng et al., 2020; Liu et al., 2023; Chen et al., 2024). Combined with the cutting relationship between fault and strata, the presence of unconformities, changes of fault slip direction, and stratigraphic sedimentary characteristics, the active stages of SB5 fault are reassessed, and four primary active stages are identified (Figure 12).

The initial active stage of the SB5 fault is identified as the Middle-Late Cambrian (Figure 12A). The manifestation of fault activity during this stage is primarily evident through the synsedimentary thickening observed within the strata of the negative flower structure deformation zone, adjacent to the $T\epsilon_3$ interface (Figure 7D), while growth strata are noted to have developed along the uplifted limb of the positive flower structure (Figure 8A). The pattern of sedimentary development indicates that the strike-slip fault was active during the late Cambrian, exerting an influence on the sedimentary feature of the strata within and surrounding the deformation zone. The presence of localized angular unconformities within the Upper Cambrian (Figure 8A) and Middle Cambrian strata (Figure 8B) suggest ongoing fault activity during the Middle to Late Cambrian. In the southern SB5 fault, the fault slip direction observed in this stage diverges from that of the Upper Ordovician (Figure 11B), further substantiating the proposition that the fault's movement initiated during the Middle and late Cambrian.

The second active stage is recognized as the Middle-Late Ordovician (Figure 12B). During this phase, the majority of the primary and branch faults associated with the strike-slip system terminated near the TO_3 interface. The activity culminated in the local uplift of the late Ordovician strata. The interface of TO_3 witnessed the most significant deformation, with growth strata prominently developing along the limb of the uplift (Figures 7C, D; Figure 8C). Additionally, unconformities are observed at the summit of the uplift (Figure 7D), indicating that the strike-slip fault was

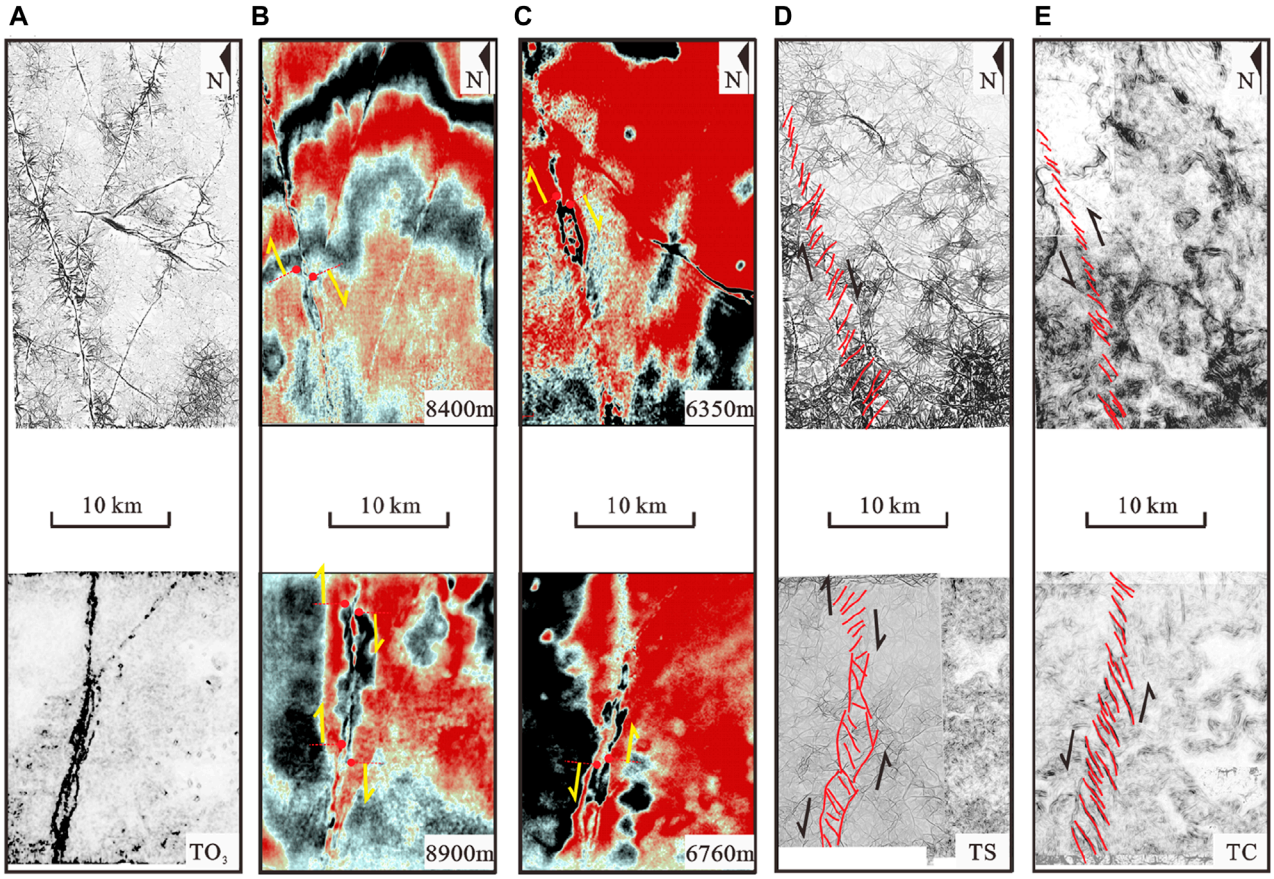

FIGURE 11
(A) Uninterpreted coherence slice of surface TO_3. **(B)** Horizontal depth slice around the surface of $T\epsilon_3$. On the $T\epsilon_3$ interface, the northern and southern SB5 fault both exhibit dextral movement. **(C)** Horizontal depth slice around the surface of TO_3. Interpreted coherence slice of surface TS **(D)** and TC **(E)**. On the TO_3 and TS interface, the northern SB5 fault maintains dextral movement, while the slip direction of southern SB5 fault changes to sinistral. On the TC interface, the northern SB5 fault undergoes a reversal, matching the slip direction of the southern SB5 fault in sinistral movement.

intensely active at the end of the Middle Ordovician and continued to the late Ordovician.

The third active stage corresponds to the Silurian (Figure 12C). In the stage, the development of the lower group echelon normal faults and boundary graben is particularly notable. These echelon normal faults terminate upward within the Silurian strata, where they are associated with the growth of synsedimentary strata. Concurrently, the boundary graben associated with the southern SB5 fault also terminate within the Silurian strata, cutting downwards through the TO_3 interface, indicating that both the echelon normal fault and the boundary graben were formed in the Silurian.

The fourth active stage spans Devonian-Carboniferous (Figure 12D). During the period, the upper group echelon normal faults were formed, and synsedimentary strata were developed within the grabens (Figures 8A, B). These faults terminate upward below the base of the Permian, which suggests that the active phase for the echelon normal faults is confined to the Devonian-Carboniferous. Furthermore, the slip directions observed at the TS and TC interfaces in the northern SB5 fault are opposite (Figures 11D, E), implies that the formation periods for the echelon normal faults differ between the upper and lower groups.

6.2 The paleostress pattern in early paleozoic

The tectonic evolution of the orogenic belts encircling the Tarim basin is notably complex, leading to a dynamically changing tectonic stress field within the basin (Lin et al., 2012; He et al., 2016). The formation and evolution of strike-slip faults within the basin are intimately related to the characteristics of the tectonic stress field (Deng et al., 2019a; Sun et al., 2021). Consequently, the reconstruction of paleo-stress field features during key tectonic periods is highly significant. By synthesizing the analysis of thrust fault development, the distribution of unconformities, the restoration of denudation processes, and the reconstruction of paleogeomorphology, extensive and detailed research has been conducted to reveal the paleo-stress field characteristics within the basin (He et al., 2011; He et al., 2016; Lin et al., 2012). However, due to limitations such as burial depth and the resolution of seismic data, the characteristics of the paleo-stress field in the early Paleozoic, particularly during the Cambrian, remain a subject of debate (Dobretsov et al., 1995; Li et al., 2013; Han et al., 2015; Han et al., 2016; Wan et al., 2018). There was a consensus that during the Cambrian, the paleo-oceans surrounding the basin were in a phase

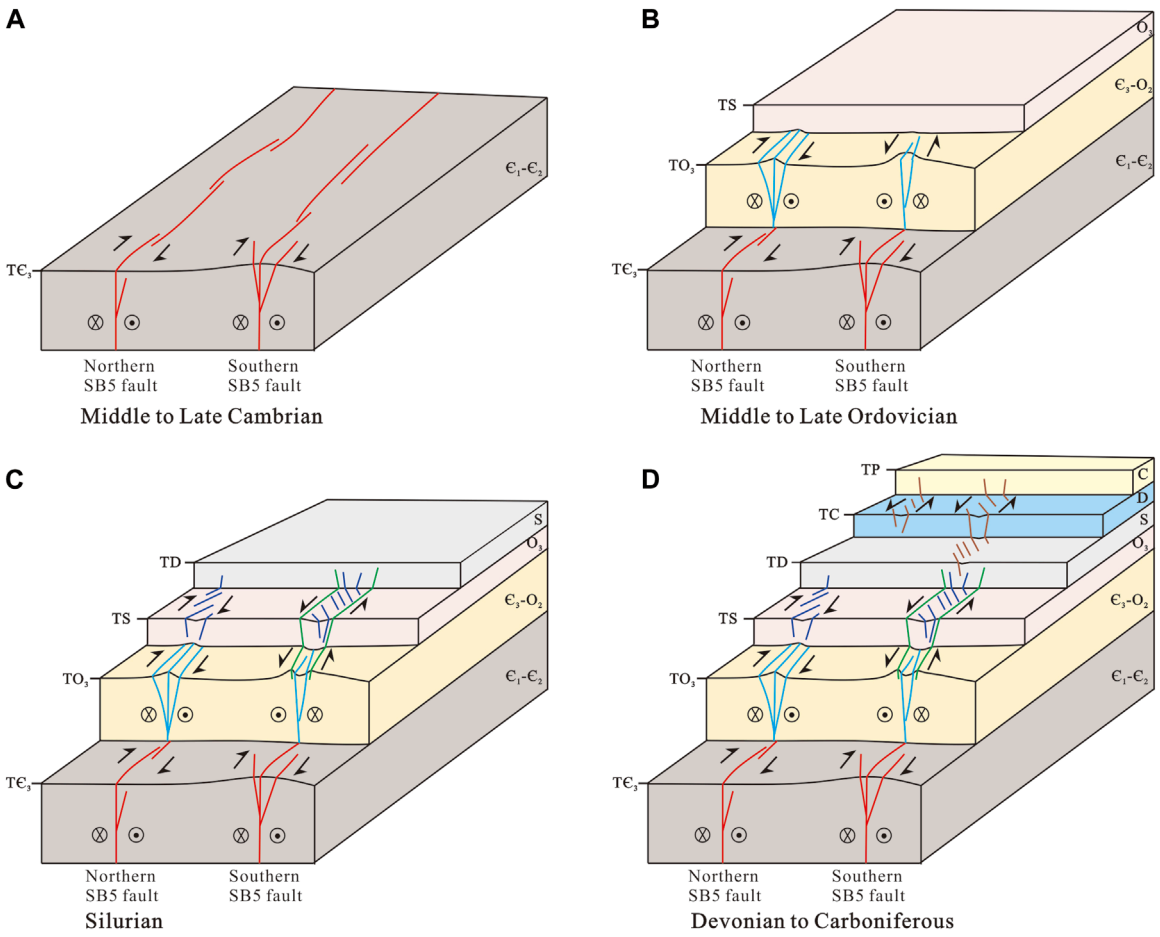

FIGURE 12
Active stages of the northern and southern SB5 strike-slip fault in Paleozoic: **(A)** Middle to late Cambrian, **(B)** Middle to Late Ordovician, **(C)** Silurian, and **(D)** Devonian to Carboniferous.

of expansion, which resulted in an extensional stress environment within the basin (Jia, 1997; Mattern and Schneider, 2000; Wang, 2004; He et al., 2016). Nevertheless, recent findings indicate that the Paleo-Asian Ocean initiated southward subduction during the Cambrian (Xu et al., 2011; Han et al., 2016). Additionally, Cambrian thrust faults have been identified in the Tazhong uplift (Chen et al., 2024), suggesting the occurrence of local compressive stress within the basin during this period.

The Cambrian to Middle Ordovician strata of the central Tarim basin display an absence of pronounced erosion. The paleotectonic characteristics of the Cambrian base ($T\epsilon_1$) during pivotal tectonic periods can be reconstructed, by calculating the thickness of strata from a crucial seismic interface down to $T\epsilon_1$. And the characteristics of the paleo-stress field at the end of the Middle Cambrian and Middle Ordovician can be estimated (Figures 13A, B), based on the paleotectonic features of $T\epsilon_1$ around the Manxi Low uplift.

At the end of the Middle Cambrian, the paleotectonic features of $T\epsilon_1$ (Figure 13A) indicate the emergence of a north-south oriented uplift in the eastern section of the Tabei uplift. Concurrently, a series of northwest-directed depressions were formed in the western of the Tabei uplift and within the Manxi Low Uplift. Additionally, folds with northwest trend were identified within the Tazhong Uplift. These paleogeomorphic features collectively imply that the Manxi Low Uplift and its adjacent regions were predominantly influenced by an east-west extensional regime at the end of the Middle Cambrian. The extensional environment resulted in a tectonic framework that exhibited east-west differentiation (Wu et al., 2021). However, the presence of localized compressive stress, oriented in a northeast-southwest direction, is suggested by the northwest alignment of the depressions and folds.

The paleotectonic features of the $T\epsilon_1$ interface at the end of the Middle Ordovician suggest a complex tectonic environment within the region. In the northern part of the Tabei Uplift, there is evidence of uplift, which transitions into a depression as moves southward (Figure 13B). The structural distribution within the Tabei-Manxi Low Uplift predominantly aligns in an east-west orientation, while the Tazhong Uplift exhibits a NWW-directed structural pattern. Notably, a localized uplift is observed in the southeast of the Tazhong Uplift. These observations indicate that the Tabei Uplift was subjected to north-south compression, while the Tazhong Uplift simultaneously experienced compressive stress from the southwest and southeast.

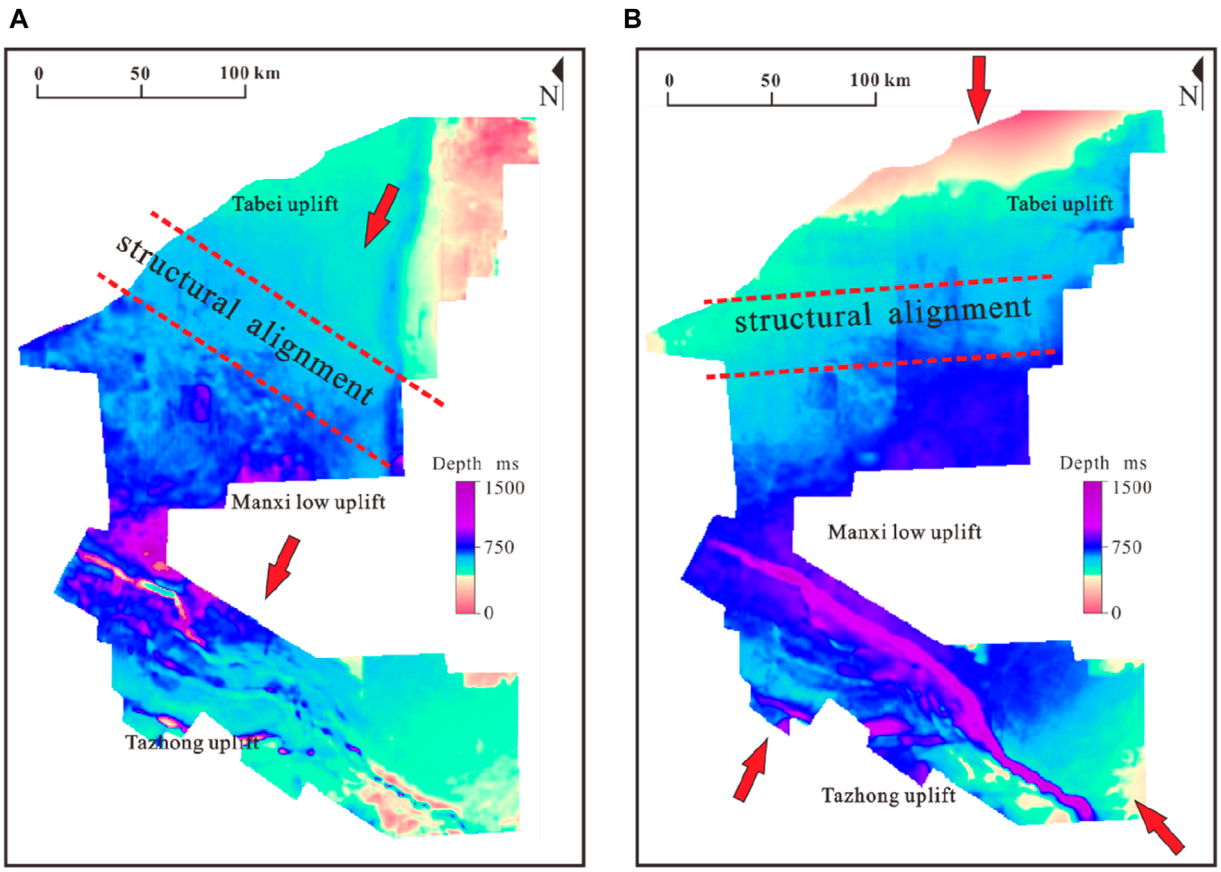

FIGURE 13
The map of paleotectonic restoration of the central Tarim basin of $T\epsilon_1$ at the end of **(A)** Middle Cambrian and **(B)** Middle Ordovician. The pleotectonic features demonstrate that Manxi low uplift and its adjacent regions were subjected to localized compressive stress in NE-SW at the end of the Middle Cambrian, and compressive stress from the north, southwest and southeast simultaneously at the end of Middle Ordovician.

Moreover, the characteristics of the unconformity within the Silurian strata of the basin further support the notion that during the Silurian, the basin was predominantly under the influence of north-south compressive stress from the northern region and southeast-directed compressive stress (He et al., 2011; He et al., 2016; Lin et al., 2012).

6.3 Basement structure characteristics of SB5 fault

Since the Tarim plate separated from the Rodinia supercontinent, it has been under intense extensional stress, a condition that has led to the extensive development of Precambrian basement rifts throughout the basin (Zhu et al., 2022a; Zhu et al., 2017; Neng et al., 2022; Chen et al., 2024). Utilizing the three-dimensional seismic data from the study area in conjunction with previous research findings (Deng et al., 2018; Deng et al., 2019a; Deng et al., 2019b; Wang et al., 2020; Sun et al., 2021; Chen et al., 2023) (Figures 14A, B), the structural characteristics of the Precambrian basement at the base of the SB5 fault are meticulously analyzed in cross sections (Figure 15). Furthermore, the geological features at the bottom of the Sinian (TZ) within the 3D surveys of Fuman Oilfield are reconstructed (Figure 14C), which is instrumental in examining the distribution pattern of the Precambrian basement rifts associated with the SB5 fault.

The distribution characteristics of the TZ within the 3D seismic surveys uncover a pronounced variation in the basement structure from east to west in the northern 3D survey area (Figure 14C). The structural orientation is predominantly north-south, with a discernible paleo-uplift in the western region and significant rifts in the eastern area. Similarly, in the central part of the southern 3D survey, a north-south oriented basement paleo-uplift is identified, flanked by rifts on either side. By superimposing the strike of the fault plane onto the basement characteristic map of the SB5 fault, a clear pattern emerges: the primary fault plane distribution closely follows the boundaries of the uplifts and rifts as identified within the 3D surveys. Moreover, the fault typically cut down the basement on the section, often located at the rim or directly overprinting the rift (Figures 15A–C).

Incorporating the findings from previous studies conducted on other segments of the SB5 fault (Deng et al., 2019a; Sun et al., 2021; Shen et al., 2022; Chen et al., 2023), the basement characteristics

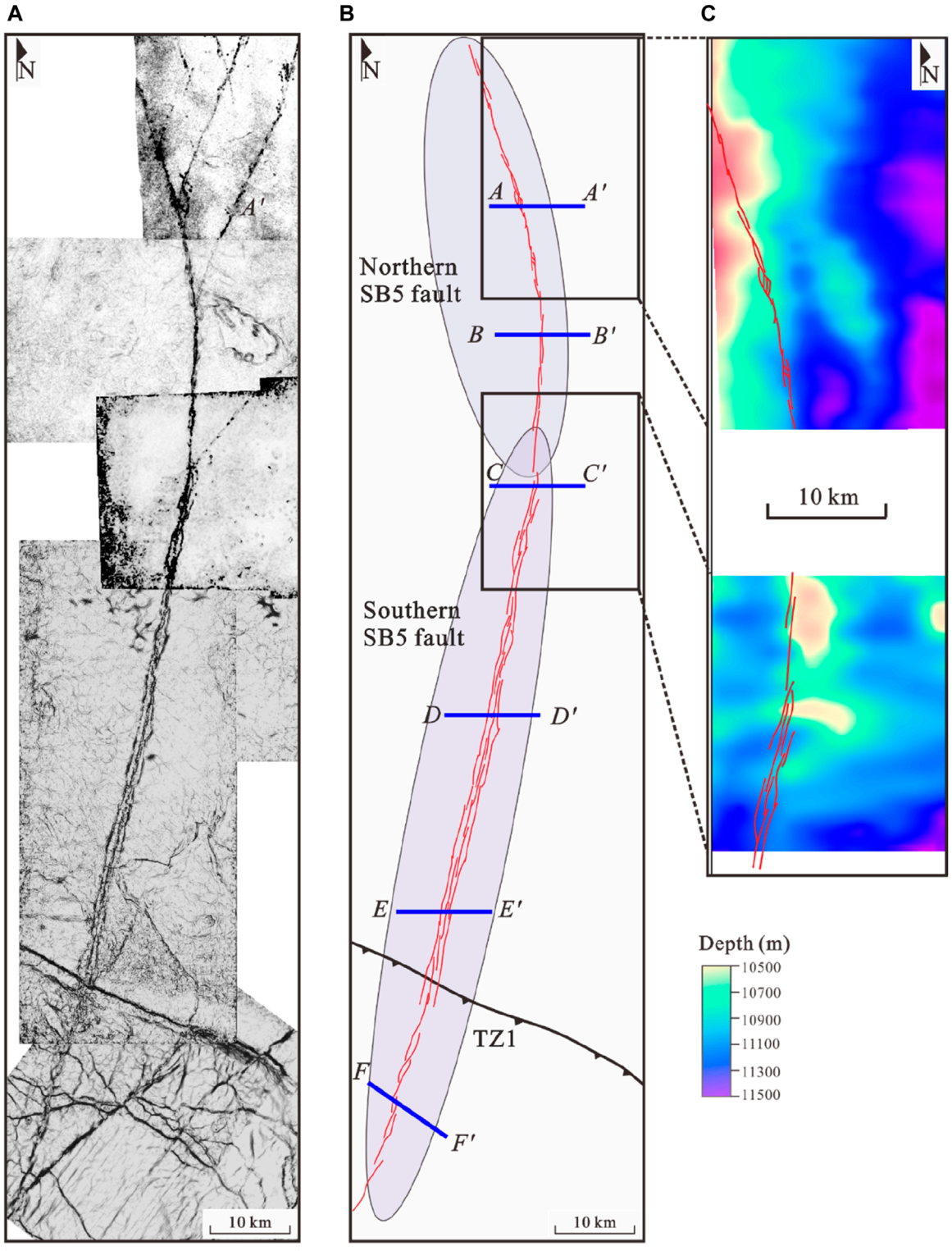

FIGURE 14
Uninterpreted **(A)** and interpreted **(B)** coherence slice of surface TO_3 (Modify from Deng et al., 2019a; Sun et al., 2021; Shen et al., 2022; Chen et al., 2023). **(C)** The depth map of surface TZ. The basement characteristic reveal that the primary fault plane distribution closely follows the boundaries of the uplift and rift as identified within the 3D surveys. (for location, see Figure 2).

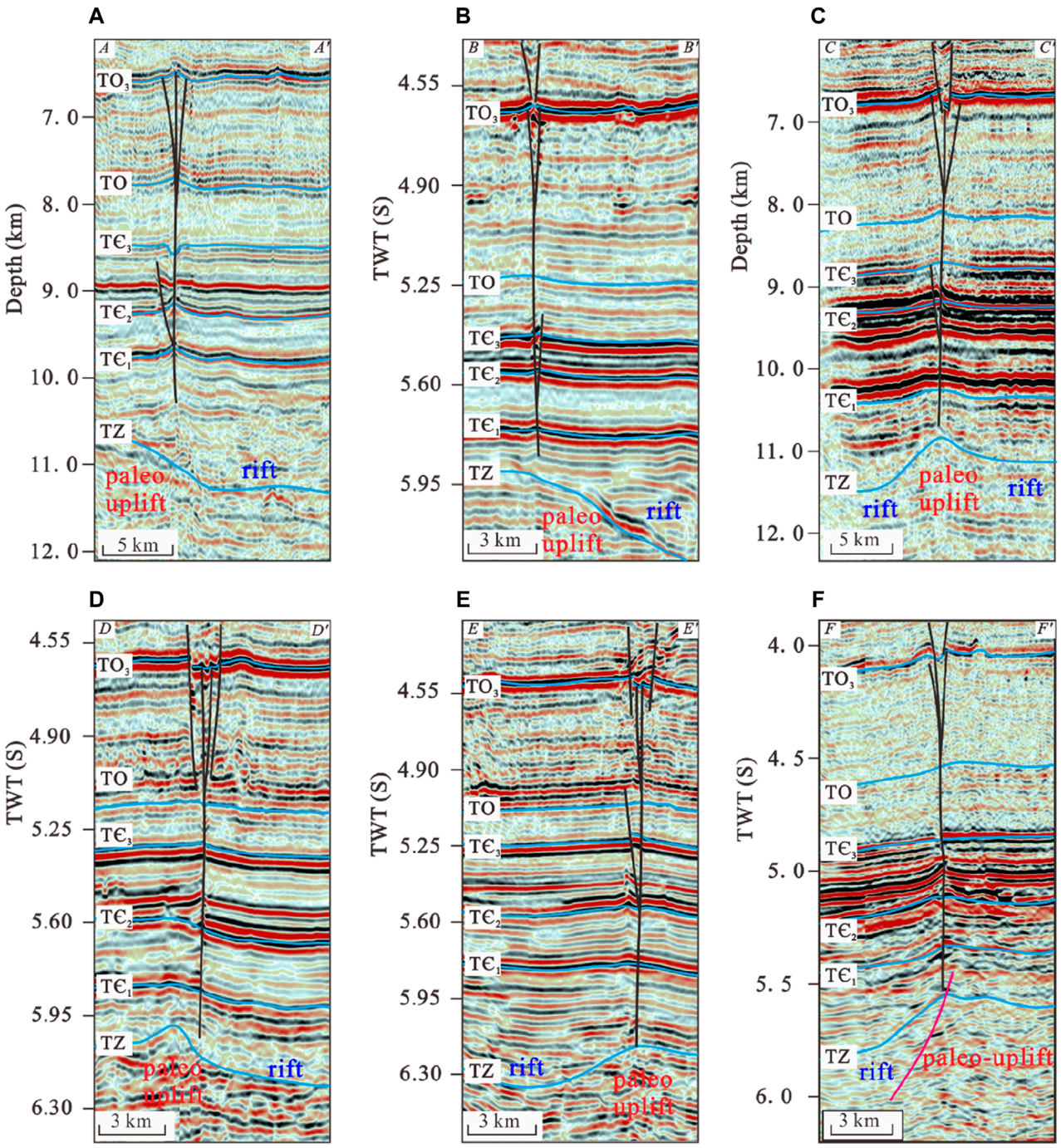

FIGURE 15
Typical seismic sections of Northern and Southern SB5 showing the basement structure **(A–F)**. The faults are predominantly situated along the margins of the rifts and are associated with the well-developed Precambrian basement rift. (for location, see Figure 14) (Sections BB′, DD′ and EE′are modified from Sun et al., 2021; Chen et al., 2023).

of the SB5 fault along the profile can be further analyzed. Along the profile, the basement characteristics of the SB5 fault in other regions exhibit similarities to those identified within the 3D survey of the Fuman Oilfield. The faults are predominantly situated along the margins of the rifts and are associated with the well-developed Precambrian basement rift (Figures 15B–F). It is reasonable to infer that the distribution of the basement rift plays a crucial role in controlling the development location of the SB5 fault, and subsequently influences the planar geometry of the fault. The strike-slip faults are more prone to rupture along rift boundaries, forming relatively short segments, which grow towards both ends and interact to connect into a complete fault.

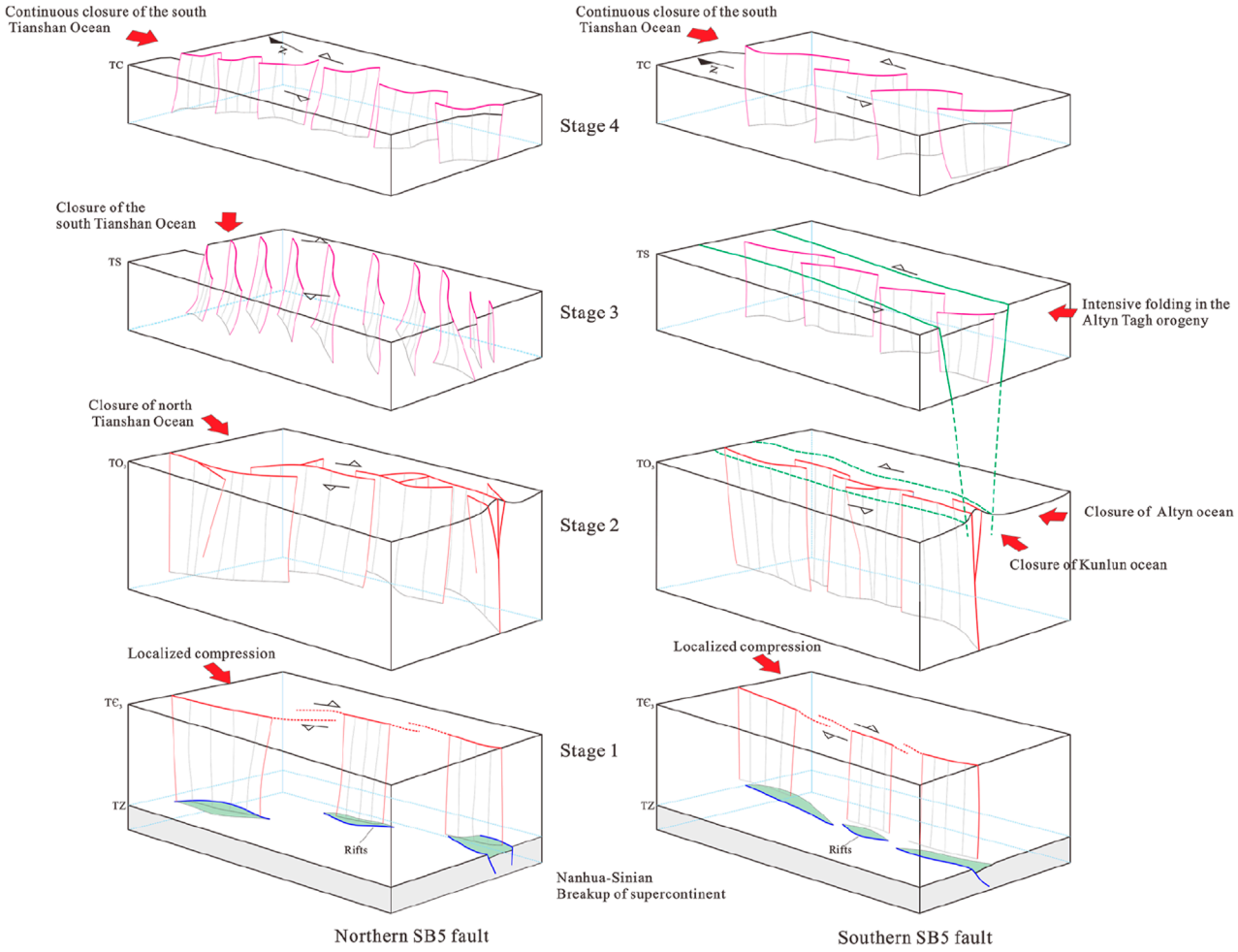

FIGURE 16
Formation mechanism and evolution processes of SB5 fault. Stage 1: embryonic stage of strike-slip activity (Middle-Late Cambrian), Stage 2: intense strike-slip fault activity stage (Middle-Late Ordovician), Stage 3: reactivation stage of deep strike-slip fault (Silurian), and Stage 4: connection and reactivation stage of the southern and northern SB5 fault (Devonian-Carboniferous).

6.4 Formation mechanism of the SB5 fault

Extensive research has been conducted on to unraveling the formation mechanisms of the SB5 fault (Deng et al., 2018; Deng et al., 2019a; Deng et al., 2019b; Lin et al., 2021; Sun et al., 2021; Chen et al., 2023). By analyzing the distribution patterns of fault slip distance and slip direction, it is generally accepted that the northern and southern SB5 faults were two separate entities during their initial stage of development, later connecting during the fault's evolution (Deng et al., 2019a; Deng et al., 2019b; Sun et al., 2021). Nonetheless, a comprehensive understanding of the formation mechanism and the specific factors that drove the significant planar deflection observed in the SB5 fault has yet to be fully established. In recent studies, some scholars have shifted their focus to the development of rifts within the basement beneath the SB5 fault (Teng et al., 2020; Shen et al., 2022), but the relationship between the distribution characteristics of these basement rifts and the formation and evolution of strike-slip faults remains unexplored.

Integrating the evolution of peripheral orogenic belts, the paleo-stress environment of the Paleozoic, the active stages of fault movement, and the characteristics of basement rifts, a model for the formation and evolution of the SB5 fault has been established (Figure 16). It outlines four key developmental stages: embryonic stage of strike-slip activity (Middle-Late Cambrian), intense strike-slip fault activity stage (Middle-Late Ordovician), reactivation stage of deep strike-slip fault (Silurian), and connection and reactivation stage of the southern and northern SB5 fault (Devonian-Carboniferous).

During the Nanhua-Sinian, the ocean around the Tarim basin was in the stage of expansion (Xu et al., 2009; Ge et al., 2014; Wu et al., 2019b), and the central Tarim basin was in extensional environment, giving rise to a series of Precambrian rift (Zhu et al., 2022a; Neng et al., 2022). During the middle and late Cambrian, the Paleo-Asian Ocean initiated southward subduction (Xu et al., 2011; Han et al., 2015; Han et al., 2016), resulting in a locally weak compressional tectonic environment within the basin (Figure 13A). Under the influence of the weak compressive

stress, oriented in the NE-SW direction from the north, the rift's margin was predisposed to vertical rupture, leading to the formation of segments with limited initial plane extension distance. These segments gradually expanded and elongated, with their planar geometry influenced by the basement rift's distribution characteristics, resulting in a counterclockwise deflection and an S-shaped distribution pattern for the SB5 fault. The northern and southern SB5 faults exhibited independent activity but both undergone dextral strike-slip movement. In the Middle-Late Ordovician, the north Tianshan Ocean's subduction beneath the central Tianshan block (Jia and Wei, 2002; Gao and Fan, 2014), along with the gradual closure of the ancient Kunlun Ocean to the southwest of the basin (Li et al., 2009; Wu et al., 2012; Lan et al., 2015), and the commencement of subduction by the Altun Ocean in the southeast beneath the Tarim plate (Lan et al., 2015; Qiu et al., 2019), led to intensive fault activity along the SB5 fault. The northern SB5 fault experienced dextral strike-slip movement due to north-south compressive stress, while the southern SB5 fault underwent sinistral strike-slip movement influenced by compressive stress from the southeast and southwest. During the Silurian, the intense folding within the Altun tectonic domain in the southeast (Liu et al., 2007), and the initiation of subduction and subsequent gradual closure of the northern South Tianshan Ocean from east to west (Chen et al., 1999; Gao and Fan, 2014), gave rise to the reactivation of the northern SB5 fault in a dextral movement under the influence of northeast compressive stress. This reactivation resulted in the formation of left-stepping en-echelon normal faults within the shallower layers. Concurrently, the southern SB5 fault, under the impact of southeast compressive stress, experienced sinistral slip, leading to the development of right-stepping en-echelon normal faults and boundary graben. During the Devonian and Carboniferous, the ongoing subduction of the south Tianshan Ocean, which ultimately closed by the end of the Carboniferous (Chen et al., 1999; Gao and Fan, 2014), led to the connection and sinistral reactivation of the southern and northern SB5 fault under the influence of NWW compressive stress from the north. The reactivation resulted in the development of right-stepping en-echelon normal faults in the shallow layers.

7 Conclusion

1. The SB5 fault demonstrates a layered deformation structure that can be categorized into three distinct structural deformation layers, discerned by their lithological and fault features. The deep structural deformation layer, beneath the $T\epsilon_3$ interface, is typified by rifts within the Precambrian basement and is associated with weak strike-slip fault activity. The middle structural deformation layer, ranging from $T\epsilon_3$ to TO_3, is marked by vigorous strike-slip faulting and the formation of a pronounced flower structure. The shallow structural deformation layer, extending from TO_3 to TP, is characterized by the emergence of normal faults in an echelon pattern, alongside the development of boundary graben in the southern SB5 fault.
2. Notable variations in fault activity are observed between the northern and southern SB5 fault across deep and shallow layers. The fault activity peaks at the TO_3 interface and is weakest at $T\epsilon_3$ interface, with the southern SB5 fault exhibiting generally larger deformational magnitude. The slip direction of the faults changes with depth. Both the northern and southern SB5 fault are dextral at $T\epsilon_3$ interface. The southern SB5 fault shifts to sinistral at TO_3 interface, and the northern SB5 fault transitions to sinistral at TC interface.
3. The formation and evolution of the SB5 fault are influenced by the distribution of Precambrian basement rifts, with fault activities spanning from the Middle Cambrian to the Carboniferous, which can be divided into four distinct tectonic evolution stages. During the Middle to Late Cambrian, the rupture of fault was concentrated along the margins of the basement rifts, leading to the initial development of the northern and southern SB5 fault. The Middle and Late Ordovician witnessed an intense upward propagation of strike-slip faults under the influence of significant compressive stress. In the Silurian, the reactivation of the underlying strike-slip faults resulted in the formation of lower group en-echelon normal faults in the shallow structural deformation layer and the development of boundary grabens in the southern SB5 fault. During the Devonian-Carboniferous, the southern and northern SB5 faults merged, with the development of upper group en-echelon normal faults in the shallow structural deformation layer.

Data availability statement

The original contributions presented in the study are included in the article/Supplementary Material, further inquiries can be directed to the corresponding author.

Author contributions

XS: Investigation, Software, Writing–original draft. SC: Conceptualization, Writing–review and editing. YZ: Supervision, Writing–review and editing. ZX: Validation, Writing–original draft. YN: Formal Analysis, Writing–original draft. XL: Methodology, Writing–original draft. PK: Funding acquisition, Writing–original draft. MY: Visualization, Writing–original draft. PC: Software, Writing–review and editing.

Funding

The author(s) declare that financial support was received for the research, authorship, and/or publication of this article. This study was financially supported by the National Natural Sciences Foundation of China (Grant No. U21B2062).

Conflict of interest

Authors YZ, ZX, and PK were employed by PetroChina Tarim Oilfield Company.

The remaining authors declare that the research was conducted in the absence of any commercial or financial relationships that could be construed as a potential conflict of interest.

Publisher's note

References

Allen, M. B., Windley, B. F., and Zhang, C. (1993). Palaeozoic collisional tectonics and magmatism of the Chinese Tienshan, central Asia. *Tectonophysics* 220 (1-4), 89–115. doi:10.1016/0040-1951(93)90225-9

Chen, C. M., Lu, H. F., Jia, D., Cai, D. S., and Wu, S. M. (1999). Closing history of the southern Tianshan oceanic basin, western China: an oblique collisional orogeny. *Tectonophysics* 302 (1-2), 23–40. doi:10.1016/s0040-1951(98)00273-x

Chen, P., Neng, Y., Wu, X., Huang, C., Wang, L. Y., and Guo, M. (2023). Stratification and segmentation characteristics and tectonic evolution of Shunbei No.5 strike-slip fault zone in Tarim Basin. *Xinjiang Petro Geo.* 44 (01), 33–42. (in Chinese with English abstract).

Chen, S., Zhang, Y. T., Xie, Z., Song, X. G., and Liang, X. X. (2024). Multi-stages of paleozoic deformation of the fault system in the Tazhong uplift, Tarim Basin, NW China: implications for hydrocarbon accumulation. *J. Asian Earth Sci.* 265, 106086. doi:10.1016/j.jseaes.2024.106086

Chen, Y. Q., Wang, X. X., He, H., and Yi, Y. (2022). Evolution of uplift and depression framework of Tarim craton in nanhua-cambrian. *China Pet. Explor.* 27 (4), 30–46.

Deng, S., Li, H. L., Han, J., Cui, D. Y., and Zou, R. (2019b). Characteristics of the central segment of Shunbei 5 strike-slip fault zone in Tarim Basin and its geological significance. *Oil Gas. Geol.* 40 (5), 990–998. (in Chinese with English abstract).

Deng, S., Li, H. L., Zhang, Z. P., Wu, X., and Zhang, J. B. (2018). Characteristics of differential activities in major strike-slip fault zones and their control on hydrocarbon enrichment in Shunbei area and its surroundings, Tarim Basin. *Oil Gas. Geol.* 39 (5), 878–888. (in Chinese with English abstract).

Deng, S., Li, H. L., Zhang, Z. P., Zhang, J. B., and Yang, X. (2019a). Structural characterization of intracratonic strike-slip faults in the central Tarim Basin. *AAPG Am. Assoc. Pet. Geol. Bull.* 103 (1), 109–137. doi:10.1306/06071817354

Deng, S., Zhao, R., Kong, Q., Li, Y., and Li, B. (2022). Two distinct strike-slip fault networks in the Shunbei area and its surroundings, Tarim Basin: hydrocarbon accumulation, distribution, and controlling factors. *AAPG Bull.* 106 (1), 77–102. doi:10.1306/07202119113

Dobretsov, N. L., Berzin, N. A., and Buslov, M. M. (1995). Opening and tectonic evolution of the Paleo-Asian ocean. *Int. Geol. Rev.* 37 (04), 335–360. doi:10.1080/00206819509465407

Dyman, T., Crovelli, R., Bartberger, C., and Takahashi, K. (2002). Worldwide estimates of deep natural gas resources based on the US Geological Survey World Petroleum Assessment 2000. *Nat. Resour. Res.* 11 (3), 207–218. doi:10.1023/a:1019860722244

Gao, J., Long, L. L., Qian, Q., Huang, D. Z., Su, W., and Reiner, K. (2006). South tianshan: a late paleozoic or a triassic orogen? Acta petrol. *Sin.* 22 (5), 1049–1061.

Gao, Z. Q., and Fan, T. L. (2014). Intra-platform tectono-sedimentary response to geodynamic transition along the margin of the Tarim Basin, NW China. *J. Asian Earth Sci.* 96, 178–193. doi:10.1016/j.jseaes.2014.08.023

Ge, R., Zhu, W., Wilde, S. A., He, J., Cui, X., Wang, X., et al. (2014). Neoproterozoic to Paleozoic long-lived accretionary orogeny in the northern Tarim Craton. *Tectonics* 33 (03), 302–329. doi:10.1002/2013tc003501

Gupta, A., and Scholz, C. H. (2000). A model of normal fault interaction based on observations and theory. *J. Struct. Geol.* 22 (7), 865–879. doi:10.1016/s0191-8141(00)00011-0

Han, B. F., He, G. Q., Wang, X. C., and Guo, Z. J. (2011). Late carboniferous collision between the Tarim and Kazakhstan-yili terranes in the western segment of the South tian Shan orogen, central asia, and implications for the northern xinjiang, western China. *Earth Sci. Rev.* 109, 74–93. doi:10.1016/j.earscirev.2011.09.001

Han, X. Y., Deng, S., Tang, L. J., and Cao, Z. C. (2017). Geometry, kinematics and displacement characteristics of strike-slip faults in the northern slope of Tazhong uplift in Tarim Basin: a study based on 3D seismic data. *Mar. Petrol. Geol.* 88, 410–427. doi:10.1016/j.marpetgeo.2017.08.033

Han, X. Y., Tang, L. J., Deng, S., and Cao, Z. C. (2020). Spatial characteristics and controlling factors of the strike-slip fault zones in the northern slope of Tazhong uplift, Tarim basin: insight from 3D seismic data. *Acta Geol. Sin. Engl. Ed.* 94 (2), 516–529. doi:10.1111/1755-6724.14333

Han, Y., Zhao, G., Cawood, P. A., Sun, M., Eizenhofer, P. R., Hou, W., et al. (2016). Tarim and North China cratons linked to northern Gondwana through switching accretionary tectonics and collisional orogenesis. *Geology* 44 (02), 95–98. doi:10.1130/g37399.1

Han, Y., Zhao, G., Sun, M., Eizenhofer, P. R., Hou, W., Zhang, X., et al. (2015). Paleozoic accretionary orogenesis in the Paleo-Asian Ocean: insights from detrital zircons from silurian to carboniferous strata at the northwestern margin of the Tarim craton. *Tectonics* 34 (02), 334–351. doi:10.1002/2014tc003668

Harding, T. P. (1974). Petroleum traps associated with wrench faults. *AAPG Bull.* 58 (7), 1290–1304. doi:10.1306/83d91669-16c7-11d7-8645000102c1865d

He, B. Z., Jiao, C. L., Xu, Z. Q., Cai, Z. H., Zhang, J. X., Liu, S. L., et al. (2016). The paleotectonic and paleogeography reconstructions of the Tarim Basin and its adjacent areas (NW China) during the late Early and Middle Paleozoic. *Gondwana Res.* 30, 191–206. doi:10.1016/j.gr.2015.09.011

He, B. Z., Xu, Z. Q., Jiao, C. L., Li, H. B., and Cai, Z. H. (2011). Tectonic unconformities and their forming: implication for hydrocarbon accumulations in Tarim basin. *Acta Pet. Sin.* 27 (01), 253–265.

He, D. F., Jia, C. Z., Li, D. S., Zhang, C. J., Meng, Q. R., and Shi, X. (2005). Formation and evolution of polycyclic superimposed Tarim Basin. Oil. *Gas. Geol.* 26 (01), 64–77. (in Chinese with English abstract).

He, D. F., Zhou, X. Y., Zhang, C. J., Yang, W. J., and Shi, X. (2006). Characteristics of geologic framework of multicycle superimposed basin in Tarim Basin. *Pet. Geol.* 11 (1), 31–41. (in Chinese with English abstract).

Jia, C. Z. (1997). *Tectonic characteristics and Petroleum, Tarim Basin. China. Pet.* Ind. Press, 1–120. (in Chinese with English abstract).

Jia, C. Z., and Wei, G. Q. (2002). Structural characteristics and petroliferous features of Tarim Basin. *Chin. Sci. Bull.* 47, 1–11. doi:10.1007/bf02902812

Jiao, F. Z. (2017). Significance of oil and gas exploration in NE strike-slip fault belts in Shuntuoguole area of Tarim Basin. *Oil Gas. Geol.* 38 (5), 831–839.

Lan, X., Lü, X., Zhu, Y., and Yu, H. (2015). The geometry and origin of strike-slip faults cutting the Tazhong low rise megaanticline (central uplift, Tarim Basin, China) and their control on hydrocarbon distribution in carbonate reservoirs. *J. Nat. Gas. Sci. Eng.* 22, 633–645. doi:10.1016/j.jngse.2014.12.030

Li, C. X., Jia, C. Z., Li, B., Yang, G., Yang, H. J., Luo, C. S., et al. (2009). Distribution and tectonic evolution of the Paleozoic fault system, the north slope of Tazhong uplift, Tarim Basin. *Acta Geol. Sin.* 83 (8), 1065–1073. (in Chinese with English abstract).

Li, C. X., Wang, X. F., Li, B. L., and He, D. F. (2013). Paleozoic fault systems of the Tazhong uplift, Tarim Basin, China. *Mar. Petrol. Geol.* 39, 48–58. doi:10.1016/j.marpetgeo.2012.09.010

Li, S. T., Ren, J. Y., Xing, F. C., Liu, Z. H., Li, H. Y., Chen, Q. L., et al. (2012). Dynamic processes of the Paleozoic Tarim basin and its significance for hydrocarbon accumulation-a review and discussion. *J. Earth Sci.* 23, 381–394. doi:10.1007/s12583-012-0262-5

Li, Y. T., Qi, L. X., Zhang, S. N., Yun, L., Cao, Z. C., Han, J., et al. (2019). Characteristics and development mode of the Middle and Lower Ordovician fault-karst reservoir in Shunbei area, Tarim basin. *Acta Pet. Sin.* 40 (12), 1470. (in Chinese with English abstract).

Li, Z. L., Chen, H. L., Song, B., Li, Y. Q., Yang, S. F., and Yu, X. (2011). Temporal evolution of the Permian large igneous province in Tarim Basin in northwestern China. *J. Asian Earth Sci.* 42, 917–927. doi:10.1016/j.jseaes.2011.05.009

Lin, B., Yun, L., Li, H. Y., Xiao, C. Y., Zhang, X., Liao, M. H., et al. (2021). Spatial structure of Shunbei No. 5 strike-slip fault and its relationship with oil and gas reservoirs in the Tarim Basin. *Oil. Gas. Geo.* 42 (06), 1344–1353. (in Chinese with English abstract).

Lin, C. S., Li, S. T., Liu, J. Y., Qian, Y. X., Luo, H., Chen, J. Q., et al. (2011). Tectonic framework and paleogeographic evolution of the Tarim basin during the Paleozoic major evolutionary stages. *Acta Petrol. Sin.* 27 (1), 210–218. (in Chinese with English abstract).

Lin, C. S., Yang, H. J., Liu, J. Y., Rui, Z. F., Cai, Z. Z., and Zhu, Y. F. (2012). Distribution and erosion of the Paleozoic tectonic unconformities in the Tarim Basin, Northwest China: significance for the evolution of paleo-uplifts and tectonic geography during deformation. *J. Asian Earth Sci.* 46, 1–19. doi:10.1016/j.jseaes.2011.10.004

Liu, Y., Suppe, J., Cao, Y. C., Hao, F., Liu, Y. D., Wang, X., et al. (2023). Linkage and formation of strike-slip faults in deep basins and the implications for petroleum accumulation: a case study from the Shunbei area of the Tarim Basin, China. *AAPG Bull.* 107 (02), 331–355. doi:10.1306/11142220110

Liu, Y. J., Neubauer, F., Genser, J., Ge, X. H., Takasu, A., Yuan, S. H., et al. (2007). Geochronology of the initiation and displacement of the Altyn strike-slip fault, western China. *J. Asian Earth Sci.* 29 (2-3), 243–252. doi:10.1016/j.jseaes.2006.03.002

Ma, D. B., Wu, G. H., Zhu, Y. F., Tao, X. W., Chen, L. X., Li, P. F., et al. (2019). Segmentation characteristics of deep strike slip faults in the Tarim Basin and its control on hydrocarbon enrichment: taking the Ordovician strike slip fault in the Halahatang Oilfield in the Tabeiarea as an example. *Earth Sci. Front.* 26 (1), 225–237. (in Chinese with English abstract).

Mann, P. (2007). Global catalogue, classification and tectonic origins of restraining- and releasing bends on active and ancient strike-slip fault systems. *Geol. Soc. Lond. Spec. Publ.* 290 (1), 13–142. doi:10.1144/sp290.2

Mattern, F., and Schneider, W. (2000). Suturing of the proto- and paleo-tethys oceans in the western Kunlun (xinjiang, China). *J. Asian Earth Sci.* 18, 637–650. doi:10.1016/s1367-9120(00)00011-0

Neng, Y., Li, Y., Qi, J. F., Ma, X., Zuo, L., and Chen, P. (2022). Deformation styles and multi-stage evolution history of a large intraplate strike-slip fault system in a paleozoic superimposed basin: a case study from the Tarim Basin, NW China. *Front. Earth Sci.* 10, 837354. doi:10.3389/feart.2022.837354

Qiu, H. B., Deng, S., Cao, Z. C., Yin, T., and Zhang, Z. P. (2019). The evolution of the complex anticlinal belt with crosscutting strike-slip faults in the central Tarim basin, NW China. *Tectonics* 38, 2087–2113. doi:10.1029/2018tc005229

Ren, J. Y., Zhang, J. X., Yang, H. Z., Hu, D. S., Li, P., and Zhang, Y. P. (2011). Analysis of fault systems in the central uplift, Tarim basin. *Acta Petrol. Sin.* 27, 219–230.

Sharps, R., McWilliams, M., Li, Y. P., Cox, A., Zhang, Z. K., Zhai, Y. J., et al. (1989). Lower Permian paleomagnetism of the Tarim block, northwestern China. *Earth Planet Sci. Lett.* 92, 275–291. doi:10.1016/0012-821x(89)90052-6

Shen, Z. Y., Neng, Y., Han, J., Huang, C., Zhu, X. X., Chen, P., et al. (2022). Structural styles and linkage evolution in the middle segment of a strike-slip fault: a case from the Tarim Basin, NW China. *J. Struct. Geol.* 157, 104558. doi:10.1016/j.jsg.2022.104558

Sun, Q. Q., Fan, T. L., Gao, Z. Q., Wu, J., Zhang, H. H., Qi, J., et al. (2021). New insights on the geometry and kinematics of the Shunbei 5 strike-slip fault in the central Tarim Basin, China. *J. Struct. Geol.* 150, 104400. doi:10.1016/j.jsg.2021.104400

Tang, L. J. (1994). Evolution and tectonic patterns of Tarim Basin. *Earth Sci.* 19 (06), 742–754.

Teng, C. Y., Cai, Z. X., Hao, F., and Cao, Z. C. (2020). Structural geometry and evolution of an intracratonic strike-slip fault zone: a case study from the north SB5 fault zone in the Tarim Basin, China. *Jorunal Struc Geo* 140, 104159. doi:10.1016/j.jsg.2020.104159

Tian, J., Yang, H. J., Zhu, Y. F., Deng, X. L., Xie, Z., Zhang, Y. T., et al. (2021). Geological conditions for hydrocarbon accumulation and key technologies for exploration and development in Fuman oilfield, Tarim Basin. *Acta Pet. Sin.* 42 (08), 971–975. (in Chinese with English abstract).

Wan, B., Li, S., Xiao, W. J., and Windley, B. F. (2018). Where and when did the Paleo-Asian ocean form? *Precambrian Res.* 317, 241–252. doi:10.1016/j.precamres.2018.09.003

Wang, Q. H., Yang, H. J., Wang, R. J., Li, S. Y., Deng, X. L., Li, Y., et al. (2021). Discovery and exploration technology of fault-controlled large oil and gas fields of ultra-deep formation in strike slip fault zone in Tarim Basin. *China Petro Exp.* 26 (04), 58–71. (in Chinese with English abstract).

Wang, Y., Chen, J., Pang, X., Wang, G., Hu, T., Zhang, B., et al. (2016). Hydrocarbon migration along fault intersection zone—a case study on Ordovician carbonate reservoirs in Tazhong area, Tarim Basin, NW China. *Geol. J.* 52 (5), 832–850. doi:10.1002/gj.2850

Wang, Z. H. (2004). Tectonic evolution of the western Kunlun orogenic belt, western China. *J. Asian Earth Sci.* 24, 153–161. doi:10.1016/j.jseaes.2003.10.007

Wang, Z. Y., Gao, Z. Q., Fan, T. L., Shang, Y. X., Qi, L. X., and Yun, L. (2020). Structural characterization and hydrocarbon prediction for the SB5M strikeslip fault zone in the Shuntuo Low Uplift, Tarim Basin. *Mar. Petroleum Geol.* 117, 104418. doi:10.1016/j.marpetgeo.2020.104418

Windley, B. F., Allen, M. B., Zhang, C., Zhao, Z. Y., and Wang, G. R. (1990). Paleozoic accretion and cenozoic redeformation of the Chinese tien Shan range, central asia. *Geology* 18 (2), 128–131. doi:10.1130/0091-7613(1990)018<0128:paacro>2.3.co;2

Wu, G. H., Chen, X., Ma, B. S., Chen, Y. Q., Tian, Z. W., Huang, S. Y., et al. (2021). The tectonic environments of the late neoproterozoic-early paleozoic and its tectono-sedimentary response in the Tarim Basin. *Acta Petrol. Sin.* 37 (08), 2431–2441. doi:10.18654/1000-0569/2021.08.11

Wu, G. H., Ga, L. H., Zhang, Y. T., Ning, C. Z., and Xie, E. (2019a). Fracture attributes in reservoir-scale carbonate fault damage zones and implications for damage zone width and growth in the deep subsurface. *J. Struct. Geol.* 118, 181–193. doi:10.1016/j.jsg.2018.10.008

Wu, G. H., Kim, Y.-S., Su, Z., Yang, P. F., Ma, D. B., and Zheng, D. M. (2020). Segment interaction and linkage evolution in a conjugate strike-slip fault system from the Tarim Basin, NW China. *Mar. Petrol. Geol.* 112, 104054. doi:10.1016/j.marpetgeo.2019.104054

Wu, G. H., Xiao, Y., He, J. Y., Chen, Z. Y., He, S., and Zhu, G. Y. (2019b). Geochronology and geochemistry of the late Neoproterozoic A-type granitic clasts in the southwestern Tarim Craton: petrogenesis and tectonic implications. *Int. Geol. Rev.* 61 (03), 280–295. doi:10.1080/00206814.2017.1423521

Wu, G. H., Yang, H. J., He, S., Cao, S. J., Liu, X., and Jing, B. (2016). Effects of structural segmentation and faulting on carbonate reservoir properties: a case study from the Central Uplift of the Tarim Basin, China. *China. Mar. Petrol. Geol.* 71, 183–197. doi:10.1016/j.marpetgeo.2015.12.008

Wu, G. H., Yang, H. J., Qu, T. L., Li, H. W., Luo, C. S., and Li, B. L. (2012). The fault system characteristics and its controlling roles on marine carbonate hydrocarbon in the Central uplift, Tarim basin. Acta Petrol. *Sin.* 28 (3), 793–805.

Wu, L., Guan, S. W., Zhang, S. C., Yang, H. J., Jin, J. Q., Zhang, X. D., et al. (2018). Neoproterozoic stratigraphic framework of the Tarim craton in NW China: implications for rift evolution. *J. Asian Earth Sci.* 158, 240–252. doi:10.1016/j.jseaes.2018.03.003

Xu, B., Xiao, S. H., Zou, H. B., Chen, Y., Li, Z. X., Song, B., et al. (2009). SHRIMP zircon U-Pb age constraints on Neoproterozoic Quruqtagh diamictites in NW China. *Precambrian Res.* 168 (3-4), 247–258. doi:10.1016/j.precamres.2008.10.008

Xu, X., Zuza, A. V., Yin, A., Lin, X. B., Chen, H. L., and Yang, S. F. (2021). Permian plume strengthened Tarim lithosphere controls the cenozoic deformation pattern of the himalayan-Tibetan orogen. *Geology* 49 (1), 96–100. doi:10.1130/g47961.1

Xu, Z. Q., Li, S. T., Zhang, J. X., Yang, J. S., He, B. Z., Li, H. B., et al. (2011). Paleo-Asian and Tethyan tectonic systems with docking the Tarim block. *Acta Petro Sin.* 27 (01), 1–22.

Yang, H. J., Chen, Y. Q., Tian, J., Du, J. H., Zhu, Y. F., Li, H. H., et al. (2020). Great discovery and its significance of ultra-deep oil and gas exploration in well Luntan-1 of the Tarim Basin. *China Petro Exp.* 25 (2), 62–72.

Yang, S. F., Chen, H. L., Ji, D. W., Li, Z. L., Dong, C. W., Jia, C. Z., et al. (2005). Geological process of early to middle Permian Magmatism in Tarim Basin and its geodynamic significance. *Geol. J. China Univ.* 11 (4), 504–511. (in Chinese with English abstract).

Yao, Y. T., Zeng, L. B., Mao, Z., Han, J., Cao, D. S., and Lin, B. (2023). Differential deformation of a strike-slip fault in the Paleozoic carbonate reservoirs of the Tarim Basin, China. *J. Struc Geo* 173, 104908. doi:10.1016/j.jsg.2023.104908

Yu, Y. X., Tang, L. J., Yang, W. J., Huang, T. Z., Qiu, N. S., and Li, W. G. (2014). Salt structures and hydrocarbon accumulations in the Tarim Basin, northwest China. *AAPG Bull.* 98, 135–159. doi:10.1306/05301311156

Yun, L. (2021). Controlling effect of NE strike-slip fault system on reservoir development and hydrocarbon accumulation in the eastern Shunbei area and its geological significance, Tarim Basin. *China Pet. Explor.* 26 (3), 41–52. (in Chinese with English abstract).

Zhang, C. L., Li, Z. X., Li, X. H., and Ye, H. M. (2009). Neoproterozoic mafic dyke swarms at the northern margin of the Tarim Block, NW China: age, geochemistry, petrogenesis and tectonic implications. *J. Asian Earth Sci.* 35, 167–179. doi:10.1016/j.jseaes.2009.02.003

Zhang, G. Y., Zhao, W. Z., Wang, H. J., Li, H. H., and Liu, L. (2007). Multicycle tectonic evolution and composite petroleum systems in the Tarim Basin. *Oil Gas. Geol.* 28, 653–663.

Zhang, Z. S., Li, M. J., and Liu, S. P. (2002). Generation and evolution of Tazhong low uplift. *Petrol. explor. Dev.* 29, 28–31.

Zheng, M. L., Wang, Y., Jin, Z. J., Li, J. C., Zhang, Z. P., Jiang, H. S., et al. (2014). Superimposition, evolution and petroleum accumulation of Tarim Basin. *Oil Gas. Geol.* 35, 925–934.

Zhu, G. Y., Chen, W. Y., Yan, H. H., Yan, L., Zhang, Z. Y., Zhao, K., et al. (2022a). Sinian tectonic evolution and distribution of source rocks in northwest Tarim Basin, China. *Mar. Petroleum Geol.* 144, 105826. doi:10.1016/j.marpetgeo.2022.105826

Zhu, G. Y., Hu, J. F., Chen, Y. Q., Xue, N., Zhao, K., Zhang, Z. Y., et al. (2022b). Geochemical characteristics and formation environment of source rock of the Lower Cambrian Yuertusi Formation in well Luntan 1in Tarim basin. *Acta Geol. Sin.* 96 (6), 2116–2130.

Zhu, G. Y., Ren, R., Chen, F. R., Li, T. T., and Chen, Y. Q. (2017). Neoproterozoic Rift basins and their control on the development of hydrocarbon source rocks in the Tarim Basin, NW China. *J. Asian Earth Sci.* 150, 63–72. doi:10.1016/j.jseaes.2017.09.018

Zhu, R. X., Zhao, P., and Zhao, L. (2022). Tectonic evolution and geodynamics of the neo-tethys ocean. *Sci. China Ear Sci.* 65 (01), 1–24. (in Chinese with English abstract). doi:10.1007/s11430-021-9845-7